

# Consistent 3D Hand Reconstruction in Video via Self-Supervised Learning

Zhigang Tu, Zhisheng Huang, Yujin Chen, Di Kang, Linchao Bao, Bisheng Yang, Junsong Yuan

**Abstract**—We present a method for reconstructing accurate and consistent 3D hands from a monocular video. We observe that detected 2D hand keypoints and the image texture provide important cues about the geometry and texture of the 3D hand, which can reduce or even eliminate the requirement on 3D hand annotation. Thus we propose  $S^2$ HAND, a self-supervised 3D hand reconstruction model, that can jointly estimate pose, shape, texture, and the camera viewpoint from a single RGB input through the supervision of easily accessible 2D detected keypoints. We leverage the continuous hand motion information contained in the unlabeled video data and propose  $S^2$ HAND(V), which uses a set of weights shared  $S^2$ HAND to process each frame and exploits additional motion, texture, and shape consistency constraints to promote more accurate hand poses and more consistent shapes and textures. Experiments on benchmark datasets demonstrate that our self-supervised approach produces comparable hand reconstruction performance compared with the recent full-supervised methods in single-frame as input setup, and notably improves the reconstruction accuracy and consistency when using video training data.

**Index Terms**—hand pose estimation, 3D hand reconstruction, video analysis, self-supervision

## 1 INTRODUCTION

HANDS play a central role in the interaction between humans and the environment, from physical contact and grasping to daily communications via hand gesture. Learning 3D hand reconstruction is the preliminary step for many computer vision applications such as augmented reality [1], sign language translation [2], [3], and human-computer interaction [4], [5], [6]. However, due to diverse hand configurations and interaction with the environment, 3D hand reconstruction remains a challenging problem, especially when the task relies on monocular data as input.

Compared with multi-view images [7], [8], [9], [10] and depth maps [11], [12], [13], [14], [15], the monocular hand images are more common in practice. In recent years, we have witnessed many efforts in recovering 3D shapes of human hands from single-view RGB images. For example, [16], [17], [18], [19], [20] were proposed to predict 3D hand pose from an RGB image. However, they only represent the 3D hand through sparse joints, and ignore the 3D shape information, which are required for some applications such as grasping objects with virtual hands [4]. To better capture the surface information of the hand, previous studies predict the triangle mesh either via regressing per-vertex coordinate [21], [22] or by deforming a parametric hand model [23], [24]. Outputting such high-dimensional representation from 2D input is challenging for neural networks to learn. As

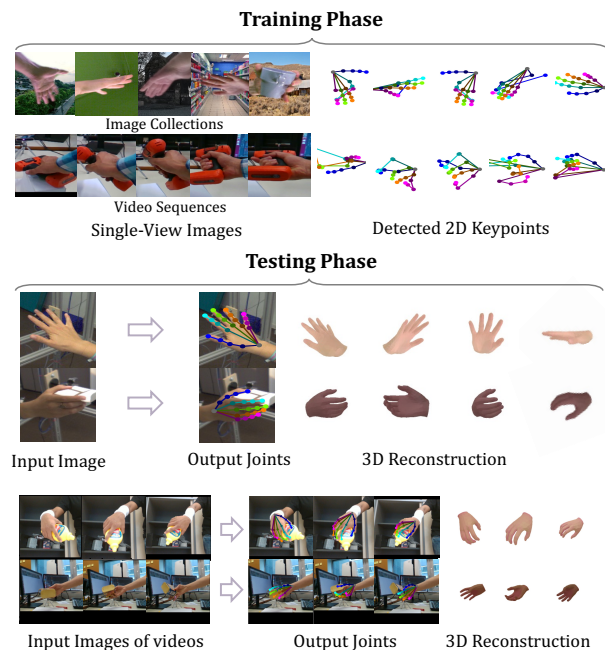


Fig. 1: Given a collection of unlabeled hand images or videos, we learn a 3D hand reconstruction network in a self-supervised manner. Top: the training uses unlabeled hand images from image collections or video sequences and their corresponding noisy detected 2D keypoints. Bottom: our model outputs accurate hand joints and shapes, as well as vivid hand textures.

- Z. Tu, Z. Huang, B. Yang are with the State Key Laboratory of Information Engineering in Surveying, Mapping and Remote Sensing, Wuhan University, Wuhan 430079, China (email: {tuzhigang, hzs5230, bshyang}@whu.edu.cn). Z. Tu and Z. Huang contributed equally and they are co-first authors.
- Y. Chen is with Technical University of Munich. Work done at Wuhan University. Correspondence to: Y. Chen (email: yujin.chen@tum.de)
- D. Kang and L. Bao are with Tencent AI Lab (email: di.kang@outlook.com, linchaobao@gmail.com).
- J. Yuan is with the Computer Science and Engineering Department, University at Buffalo, Buffalo, NY 14228, USA (email: jsyuan@buffalo.edu).

a result, the training process relies heavily on 3D hand annotations such as dense hand scans, model-fitted parametric hand mesh, or human-annotated 3D joints. Besides, the hand texture is important in some applications, such as vivid hands reconstruction in immersive virtual reality. But only recent work try to explore parametric texture estimation in a learning-based hand recovery system [25], while most previous work of 3D hand reconstruction do not

consider texture modeling [25].

One of our key observations is that the 2D cues in the hand image are quite informative to reconstruct the 3D hand model in the real world. The 2D hand keypoints contain rich structural information, and the 2D image contains abundant texture and shape information. Both are important for reducing the use of expensive 3D annotations but have not been fully investigated. Leveraging these cues, we could directly use 2D annotations and the input image to learn the geometry and texture representations without relying on 3D annotations [19]. However, it is still labor-consuming to annotate 2D hand keypoints per image. To completely save the manual annotation, we propose to extract 2D hand keypoints as well as geometric representations from the unlabeled hand image to help the shape reconstruction and use the texture information contained in the input image to help the texture modeling.

Additionally, video sequences contain rich hand motion and more comprehensive appearance information. Usually, a frame-to-frame fully-supervised hand reconstruction model does not take these information into serious consideration since 3D annotations already provide a strong supervision. As a result, it is more difficult for a frame-to-frame model to produce consistent results from video frames compared to sequence-to-sequence models, since no temporal information is utilized. Thereby, we propose to penalize the inconsistency of the output hand reconstructions from consecutive observations of the same hand. In this way, motion prior in video is distilled in the frame-to-frame model to help reconstruct more accurate hand for every single frame. Notably, the constraints on the sequence output are also employed in a self-supervised manner.

Driven by the above observations, this work aims to train an accurate 3D hand reconstruction network using only the supervision signals obtained from the input images or video sequences while eliminating manual annotations of the training images. To this end, we use an off-the-shelf 2D keypoint detector [26] to generate some noisy 2D keypoints, and supervise the hand reconstruction by these noisy detected 2D keypoints and the input image. Further, we leverage the self-supervision signal embedded in the video sequence to help the network produce more accurate and temporally more coherent hand reconstructions. To learn in a self-supervised manner, there are several issues to be addressed. First, how to efficiently use joint-wise 2D keypoints to supervise the ill-posed monocular 3D hand reconstruction? Second, how to handle noise in the 2D detection output since our setting is without utilizing any ground truth annotation? Third, is it possible to make use of the continuous information contained in video sequences to encourage smoothness and consistency of reconstructed hands in a frame-to-frame model?

To address the first issue, a model-based autoencoder is learned to estimate 3D joints and shape, where the output 3D joints are projected into 2D image space and forced to align with the detected keypoints during training. However, if we only align keypoints in image space, invalid hand pose often occurs. This may be caused by an invalid 3D hand configure which is still compatible with the projected 2D keypoints. Furthermore, 2D keypoints cannot reduce the scale ambiguity of the predicted 3D hand. Thus, we propose

to learn a series of priors embedded in the model-based hand representations to help the neural network output hand with a reasonable pose and size.

To address the second issue, a trainable 2D keypoint estimator and a novel 2D-3D consistency loss are proposed. The 2D keypoint estimator outputs joint-wise 2D keypoints and the 2D-3D consistency loss links the 2D keypoint estimator and the 3D reconstruction network to make the two mutually beneficial to each other during the training. In addition, we find that the detection accuracy of different samples varies greatly, thus we propose to distinguish each detection item to weigh its supervision strength accordingly.

To address the third issue, we decompose the hand motion into the joint rotations and ensure smooth rotations of hand joints between frames by conforming to a quaternion-based representation. Furthermore, a novel quaternion loss function is proposed to allow all possible rotation speeds. Besides motion consistency, hand appearance is another main concern. A T&S (texture and shape) consistency loss function is introduced to regularize the coherence of the output hand texture and shape.

In brief, we present a self-supervised 3D hand reconstruction ( $S^2$ HAND) model and its advanced  $S^2$ HAND(V). The models enable us to train neural networks that can predict 3D pose, shape, texture and camera viewpoint from images without any ground truth annotation of training images, except that we use the outputs from a 2D keypoint detector (see Fig. 1). Notably,  $S^2$ HAND(V) is able to extract informative supervision from unannotated videos to help learn a better frame-to-frame model. In order to achieve this,  $S^2$ HAND(V) inputs the sequential data to multiple weight-shared  $S^2$ HAND models and employs proposed constraints on the sequential output at the training stage.

The advantage of our proposed methods are summarized as follows:

- We present the first self-supervised 3D hand reconstruction models, which accurately outputs 3D joints, mesh, and texture from a single image, without using any annotated training data.
- We exploit an additional trainable 2D keypoint estimator to boost the 3D reconstruction through a mutual improvement manner, in which a novel 2D-3D consistency loss is constructed.
- We introduce a hand texture estimation module to learn vivid hand texture via self-supervision.
- We benchmark self-supervised 3D hand reconstruction on some currently challenging datasets, where our self-supervised method achieves comparable performance to previous fully-supervised methods.

This work is an extension of our conference paper [27]. The new contributions include:

- We extend our  $S^2$ HAND model to the  $S^2$ HAND(V) model, which further exploits the self-supervision signals embedded in video sequences without adopting additional temporal modules. The improvement in accuracy and smoothness is 3.5% and 3.1% respectively, measured in MPJPE and ACC.
- We present a quaternion loss function, which is based on an explored motion-aware joints rotation repre-

sentation, to help learn smooth hand motion. Experiments demonstrate its significant advantage over similar methods in both accuracy and smoothness.

- We propose a texture and shape consistency regularization term to encourage coherent shape and texture reconstruction.
- We illustrate that utilizing extra in-the-wild unlabeled training data can further boost the performance of our model.

## 2 RELATED WORK

**Hand Pose and Shape Estimation.** Researchers have developed a lot of different methods in hand pose and shape estimation, such as regression-based method [20], [28], [29], [30], [31] and model-based method [32], [33], [34], [35]. Comparing to hand pose which is represented by 3D coordinates of hand joints alone, hand mesh contains more detailed shape information and recently has become the focus in the research community. Several methods utilize the hand mesh topology to directly output 3D mesh vertices. E.g. [36], [37], [38] use the spiral convolution to recover hand mesh and [30], [39], [40] use the graph convolution to output mesh vertices. Although these methods introduce as few priors as possible, they require large amounts of annotated data for training. In this self-supervised work, we make use of the priors contained in the MANO hand model [41], where MANO can map pose and shape parameters to a triangle mesh [24], [42], [43], [44], to reduce reliance on the labeled training data.

Because the parametric model contains abundant structure priors of human hands, recent works integrate hand model as a differentiable layer in neural networks [23], [24], [42], [44], [45], [46], [47], [48]. Among them, [45], [47], [48] output a set of intermediate estimations, like segmentation mask and 2D keypoints, and then map these representations to the MANO parameters. Different from them, we aim at demonstrating the feasibility of a self-supervised framework using an intuitive autoencoder. We additionally output 2D keypoint estimation from another branch and utilize it only during training to facilitate 3D reconstruction. More generally, recent methods [23], [24], [42], [44], [46] directly adopt an autoencoder that couples an image feature encoding stage with a model-based decoding stage. Unlike [23], [24], we focus on hand recovery and do not use any annotation about objects. More importantly, the above methods use 3D annotations as supervision, while the proposed method does not rely on any ground truth annotations.

**3D Hand Pose and Shape Estimation with Limited Supervision.** 2D annotation is cheaper than 3D annotation, but it is difficult to deal with the ambiguity of depth and scale. [17] uses a depth map to perform additional weak supervision to strengthen 2D supervision. [19] proposes the biomechanical constraints to help the network output feasible 3D hand configurations. [49] detects 2D hand keypoints and directly fits a hand model to the 2D detection. [22] gathers a large-scale dataset through an automated data collection method similar to [49] and then applies the collected mesh as supervision. In this work, we limit biomechanical feasibility by introducing a set of constraints on the skin model instead of only imposing constraints on

the skeleton as [19]. In contrast to [17], [22], our method is designed to verify the feasibility of (noisy) 2D supervision and avoids introducing any extra 2.5D or 3D data.

**Self-supervised 3D Reconstruction.** Recently, there are methods that propose to learn 3D geometry from the monocular image only. For example, [50] presents an unsupervised approach to learn 3D deformable objects from raw single-view images, but they assume the object is perfectly symmetric, which is not the case in the hand reconstruction. [51] removes out keypoints from the supervision signals, but it uses ground truth 2D silhouette as supervision and only tackles categories with small intra-class shape differences, such as birds, shoes, and cars. [52] explores a depth-based self-supervised 3D hand pose estimation method, but the depth image provides much more strong evidence and supervision than the RGB image. Recently, [53], [54], [55] exploits a self-supervised face reconstruction method with the usage of 3D morphable model of face (3DMM) [56] and 2D landmarks detection. Our approach is similar to them, but the hand is relatively non-flat and asymmetrical when compared with the 3D face, and the hand suffers from more severe self-occlusion. These characteristics make this self-supervised hand reconstruction task more challenging.

**Texture Modeling in Hand Recovery.** [57], [58] exploit shading and texture information to handle the self-occlusion problem in the hand tracking system. Recently, [25] uses principal component analysis (PCA) to build a parametric texture model of hand from a set of textured scans. In this work, we try to model texture from self-supervised training without introducing extra data, and further investigate whether the texture modeling helps with the shape modeling.

**Motion Learning from Sequence Data for 3D Hand Estimation.** To leverage motion information contained in sequence data, several methods have been proposed in hand pose estimation. [23] uses the photometric consistency between neighboring frames of sparsely annotated RGB videos. [59] presents a graph-based method to exploit spatial and temporal relationship for sequence pose estimation. [32], [60] design a temporal consistency loss for motion smoothness. However, these methods either are specialized for motion generation or only impose a weak regularization for motion smoothness. There exists no approach to capture hand motion dynamics fundamentally, leading to limited benefits can be gained from modeling motion. In this work, we aim to exploit self-supervised information from hand motion dynamics. Unlike most of the previous approaches [61], [62], [63], [64] which adopt recurrent or graph-based network structure to learn hand motion in a sequence-to-sequence manner, we instead use a motion-related loss function to help our frame-to-frame model converges better and bridges the gap with fully-supervised methods.

From the above analysis and comparison, we believe that self-supervised 3D hand reconstruction is feasible and significant, but to the best of our knowledge, no such idea has been studied in this field. In this work, we fill this gap and propose the first self-supervised 3D hand reconstruction model, and prove its effectiveness through extensive experiments.

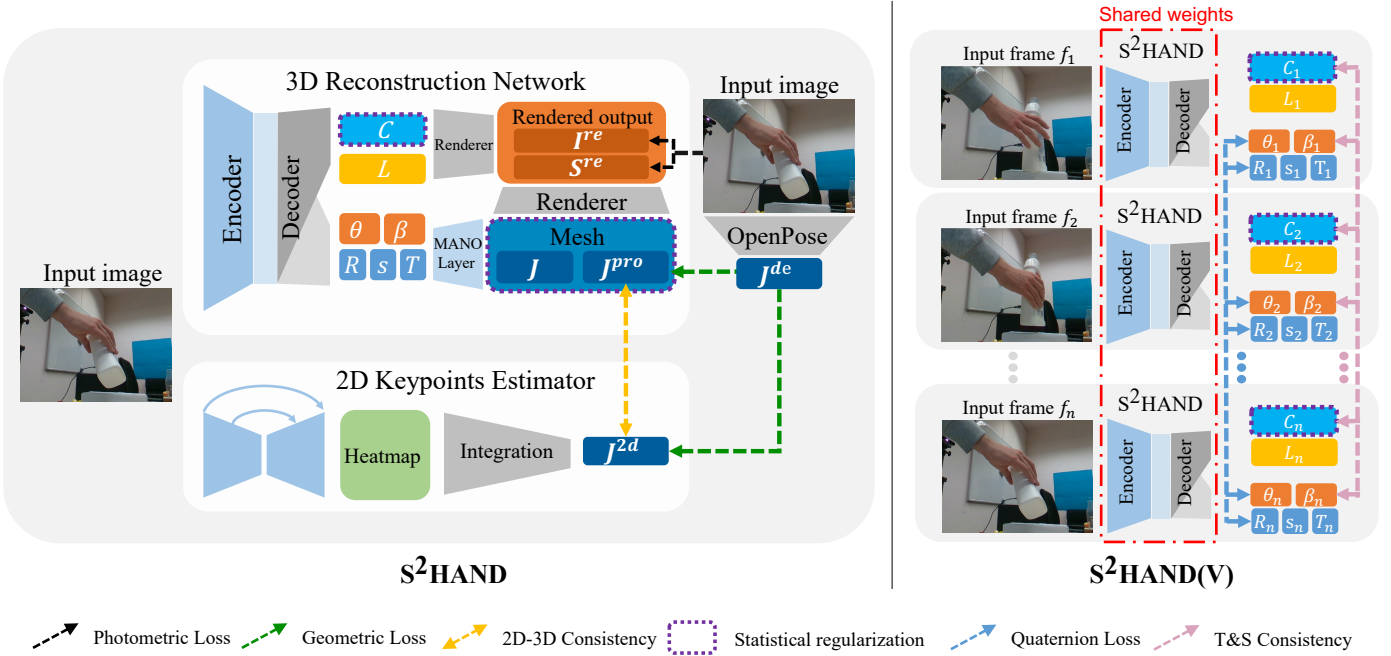


Fig. 2: Overview of the proposed method. The S<sup>2</sup>HAND(V) on the right learns to reconstruct consistent 3D hands from video sequences without ground truth annotations based on S<sup>2</sup>HAND. Given an input image, the S<sup>2</sup>HAND model generates a 3D textured hand with its corresponding multiple 2D representations through a 3D reconstruction network and a 2D keypoints estimator. Effective loss functions and regularization terms are designed for self-supervised network training. Given a video sequence, the S<sup>2</sup>HAND(V) model produces sequential outputs from several weight-shared S<sup>2</sup>HAND models with temporal constraints. A quaternion loss and a T&S loss are presented to exploit continuous motion information to promote consistent hand reconstruction. During the inference, only the 3D reconstruction network is utilized and the S<sup>2</sup>HAND(V) acts just like a specially trained S<sup>2</sup>HAND due to weight sharing. The symbols used in this figure can be found in Section 3.2 and Section 3.3.

### 3 METHODOLOGY

#### 3.1 Overview

Our method enables end-to-end learning of accurate and consistent 3D hand reconstruction from video sequences in a self-supervised manner through S<sup>2</sup>HAND(V) (Section 3.3), which is based on S<sup>2</sup>HAND (Section 3.2). The overview is illustrated in Fig. 2.

The S<sup>2</sup>HAND model takes an image as input and generates a textured 3D hand represented by pose, shape and texture, along with corresponding lighting, camera viewpoint (Section 3.2.1 and 3.2.2) and multiple 2D representations in the image space (Section 3.2.3). Some valid loss functions and regularization terms (Section 3.2.4) are explored to train the network without using ground truth annotations. The S<sup>2</sup>HAND(V) model takes video sequences as input and produces consistent sequential outputs from multiple S<sup>2</sup>HAND models where their weights are shared. A quaternion loss (Section 3.3.1) and a T&S consistency loss (Section 3.3.2) are designed to train the network with temporal constraints. We describe the proposed method in detail as below.

#### 3.2 Self-supervised Hand Reconstruction from image collections

The S<sup>2</sup>HAND model learns self-supervised 3D hand reconstruction from image collections via training a 3D hand reconstruction network with the help of a 2D keypoints estimator.

##### 3.2.1 Deep Hand Encoding

Given a image  $I$  contains a hand, the 3D hand reconstruction network first uses an EfficientNet-b0 backbone [65] to

encode the image into a geometry semantic code vector  $x$  and a texture semantic code vector  $y$ . The geometry semantic code vector  $x$  parameterizes the hand pose  $\theta \in \mathbb{R}^{30}$ , shape  $\beta \in \mathbb{R}^{10}$ , scale  $s \in \mathbb{R}^1$ , rotation  $R \in \mathbb{R}^3$  and translation  $T \in \mathbb{R}^3$  in a unified manner:  $x = (\theta, \beta, s, R, T)$ . The texture semantic code vector  $y$  parameterizes the hand texture  $C \in \mathbb{R}^{778 \times 3}$  and scene lighting  $L \in \mathbb{R}^{11}$  in a unified manner:  $y = (C, L)$ .

##### 3.2.2 Model-based Hand Decoding

Given the geometry semantic code vector  $x$  and the texture semantic code vector  $y$ , our model-based decoder generates a textured 3D hand model in the camera space. In the following, we will detailedly describe the used hand model and decoding network.

**Pose and Shape Representation.** The hand surface is represented by a manifold triangle mesh  $M \equiv (V, F)$  with  $n = 778$  vertices  $V = \{v_i \in \mathbb{R}^3 | 1 \leq i \leq n\}$  and faces  $F$ . The faces  $F$  indicates the connection of the vertices in the hand surface, where we assume the face topology keeps fixed. Given the mesh topology, a set of  $k = 21$  joints  $J = \{j_i \in \mathbb{R}^3 | 1 \leq i \leq k\}$  can be directly formulated from the hand mesh. Here, the hand mesh and joints are recovered from the pose vector  $\theta$  and the shape vector  $\beta$  via MANO, where MANO is a low-dimensional parametric model [41].

**3D Hand in Camera Space.** After representing 3D hand via MANO hand model from pose and shape parameters, the mesh and joints are located in the hand-relative coordinate systems. To represent the output joints and mesh in the camera coordinate system, we use the estimated scale,

rotation and translation to conserve the original hand mesh  $M_0$  and joints  $J_0$  into the final representations in terms of:  $M = sM_0R + T$  and  $J = sJ_0R + T$ .

**Texture and Lighting Representation.** We use per-vertex RGB value of  $n = 778$  vertices to represent the texture of hand  $C = \{c_i \in \mathbb{R}^3 | 1 \leq i \leq n\}$ , where  $c_i$  yields the RGB values of vertex  $i$ . In our model, we use a simple ambient light and a directional light to simulate the lighting conditions [66]. The lighting vector  $L$  parameterizes ambient light intensity  $l^a \in \mathbb{R}^1$ , ambient light color  $l_c^a \in \mathbb{R}^3$ , directional light intensity color  $l^d \in \mathbb{R}^1$ , directional light color  $l_c^d \in \mathbb{R}^3$ , and directional light direction  $n^d \in \mathbb{R}^3$  in a unified representation:  $L = (l^a, l_c^a, l^d, l_c^d, n^d)$ .

### 3.2.3 Represent Hand in 2D Space

A set of estimated 3D joints within the camera scope can be projected into the image space by camera projection. Similarly, the output textured model can be formulated into a realistic 2D hand image through a neural renderer. In addition to the 2D keypoints projected from the model-based 3D joints, we can also estimate the 2D position of each keypoint in the input image. Here, we represent 2D hand with three modes and explore the complementarity among them.

**Joints Projection.** Given a set of 3D joints in camera coordinates  $J$  and the intrinsic parameters of the camera, we use camera projection  $\Pi$  to project 3D joints into a set of  $k = 21$  2D joints  $J^{pro} = \{j_i^{pro} \in \mathbb{R}^2 | 1 \leq i \leq k\}$ , where  $j_i^{pro}$  yields the position of the  $i$ -th joint in image UV coordinates:  $J^{pro} = \Pi(J)$ .

**Image Formation.** A 3D mesh renderer is used to conserve the triangle hand mesh into a 2D image, here we use the implementation<sup>1</sup> of [66]. Given the 3D mesh  $M$ , the texture of the mesh  $C$  and the lighting  $L$ , the neural renderer  $\Delta$  can generate a silhouette of hand  $S^{re}$  and a color image  $I^{re}$ :  $S^{re}, I^{re} = \Delta(M, C, L)$ .

**Extra 2D Joint Estimation.** Projecting model-based 3D joints into 2D can help the projected 2D keypoints retain the structural information, but at the same time gives up the independence of each key point. To address this issue,, we additionally use a 2D keypoint estimator to directly estimate a set of  $k = 21$  independent 2D joints  $J^{2d} = \{j_i^{2d} \in \mathbb{R}^2 | 1 \leq i \leq k\}$ , where  $j_i^{2d}$  indicates the position of the  $i$ -th joint in image UV coordinates. In our 2D keypoint estimator, a stacked hourglass network [67] along with an integral pose regression [68] is used. Note that the 2D hand pose estimation module is optionally deployed in the training period and is not required during the inference.

### 3.2.4 Training Objective

Our overall training loss  $E_{S^2HAND}$  consists of three parts, i.e. a 3D branch loss  $E_{3d}$ , a 2D branch loss  $E_{2d}$  and a 2D-3D consistency loss  $E_{con}$ :

$$E_{S^2HAND} = w_{3d}E_{3d} + w_{2d}E_{2d} + w_{con}E_{con} \quad (1)$$

Note,  $E_{2d}$  and  $E_{con}$  are optional and only used when the 2D estimator is applied. The constant weights  $w_{3d}$ ,  $w_{2d}$  and  $w_{con}$  balance the three terms. In the following, we describe these loss terms in detail.

To train the model-based 3D hand decoder, we enforce geometric alignment  $E_{geo}$ , photometric alignment  $E_{photo}$  and statistical regularization  $E_{regu}$ :

$$E_{3d} = w_{geo}E_{geo} + w_{photo}E_{photo} + w_{regu}E_{regu} \quad (2)$$

**Geometric Alignment.** We propose a geometric alignment loss  $E_{geo}$  based on the detected 2D keypoints which are obtained through an implementation<sup>2</sup> of [26]. The detected 2D keypoints  $L = \{(j_i^{de}, con_i) | 1 \leq i \leq k\}$  allocate each keypoint with a 2D position  $j_i^{de} \in \mathbb{R}^2$  and a 1D confidence  $con_i \in [0, 1]$ . The geometric alignment loss in the 2D image space consists of a joint location loss  $E_{loc}$  and a bone orientation loss  $E_{ori}$ . The joint location loss  $E_{loc}$  enforces the projected 2D keypoints  $J^{pro}$  to be close to its corresponding 2D detections  $J^{de}$ , and the bone orientation loss  $E_{ori}$  enforces the  $m = 20$  bones of the keypoints in these two sets to be aligned:

$$E_{loc} = \frac{1}{k} \sum_{i=1}^k con_i \mathcal{L}_{SmoothL1}(j_i^{de}, j_i^{pro}) \quad (3)$$

$$E_{ori} = \frac{1}{m} \sum_{i=1}^m con_i^{bone} \| \nu_i^{de} - \nu_i^{pro} \|_2^2 \quad (4)$$

Here, a SmoothL1 loss [69] is used in Eq. 3 to make the loss term to be more robust to local adjustment since the detection keypoints are not fit well with the MANO keypoints. In Eq. 4,  $\nu_i^{de}$  and  $\nu_i^{pro}$  are the normalized  $i$ -th bone vector of the detected 2D joints and the projected 2D joints, respectively, and  $con_i^{bone}$  is the product of the confidence of the two detected 2D joints of the  $i$ -th bone. The overall geometric alignment loss  $E_{geo}$  is the weighted sum of  $E_{loc}$  and  $E_{ori}$  with a weighting factor  $w_{ori}$ :

$$E_{geo} = E_{loc} + w_{ori}E_{ori} \quad (5)$$

**Photometric Consistency.** For the image formation, the ideal result is the rendered color image  $I^{re}$  matches the foreground hand of the input  $I$ . To this end, we employ a photometric consistency which has two parts: the pixel loss  $E_{pixel}$  is computed by averaging the least absolute deviation (L1) distance for all visible pixels to measure the pixel-wise difference, and the structural similarity (SSIM) loss  $E_{SSIM}$  is estimated by evaluating the structural similarity between the two images [70]:

$$E_{pixel} = \frac{con_{sum}}{|S^{re}|} \sum_{(u,v) \in S^{re}} \| I_{u,v} - I_{u,v}^{re} \|_2 \quad (6)$$

$$E_{SSIM} = 1 - SSIM(I \odot S^{re}, I^{re}) \quad (7)$$

Here, the rendered silhouette  $S^{re}$  is used to get the foreground part of the input image for loss computation. In Eq. 6, we use  $con_{sum}$ , which is the sum of the detection confidence of all keypoints, to distinguish different training samples. This is because we think that low-confidence samples correspond to ambiguous texture confidence, e.g., the detection confidence of an occluded hand is usually low. The photometric consistency loss  $E_{photo}$  is the weighted sum of  $E_{pixel}$  and  $E_{SSIM}$  with a weighting factor  $w_{SSIM}$ :

$$E_{photo} = E_{pixel} + w_{SSIM}E_{SSIM} \quad (8)$$

1. [https://github.com/daniilidis-group/neural\\_renderer](https://github.com/daniilidis-group/neural_renderer)

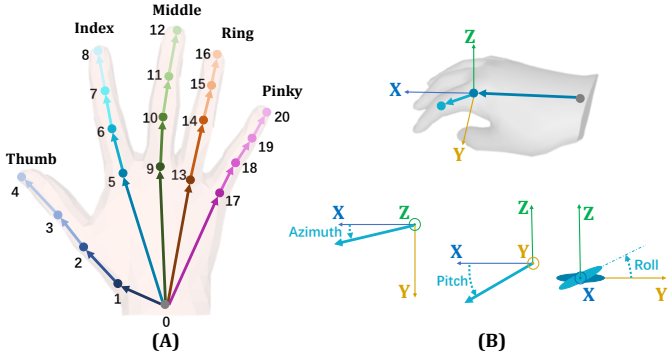


Fig. 3: (A)The joint skeleton structure. (B) A sample of bone rotation angles. The five bones  $(\vec{01}, \vec{03}, \vec{09}, \vec{013}, \vec{017})$  on the palm are fixed. Each finger has 3 bones, and the relative orientation of each bone from its root bone is represented by azimuth, pitch, and roll.

**Statistical Regularization.** During training, to make the results plausible, we introduce some regularization terms, including the shape regularization  $E_\beta$ , the texture regularization  $E_C$ , the scale regularization  $E_s$ , and the 3D joints regularization  $E_J$ . The shape regularization term is defined as  $E_\beta = \|\beta - \bar{\beta}\|$  to encourage the estimated hand model shape  $\beta$  to be close to the average shape  $\bar{\beta} = \vec{0} \in \mathbb{R}^{10}$ . The texture regularization  $E_C$  is used to penalize outlier RGB values. The scale regularization term  $E_s$  is used to ensure the output hand has appropriate size, so as to help determining the depth of the output in this monocular 3D reconstruction task. To enforce the regularizations on skeleton  $E_J$ , we define feasible range for each rotation angle  $a_i$  (as shown in Fig. 3B) and penalize those who exceed the feasible threshold. To know more details about  $E_C$ ,  $E_s$  and  $E_J$ , please refer to the Appendix of our conference paper [27].

The statistical regularization  $E_{regu}$  is the weighted sum of  $E_\beta$ ,  $E_C$ ,  $E_s$  and  $E_J$  with weighting factors  $w_C$ ,  $w_s$  and  $w_J$ :

$$E_{regu} = E_\beta + w_C E_C + w_s E_s + w_J E_J \quad (9)$$

**2D Branch Loss.** For the 2D keypoint estimator, we use a joint location loss as Eq. 3 with replacing the projected 2D joint  $j_i^{pro}$  by the estimated 2D joint  $j_i^{2d}$ :

$$E_{2d} = \frac{1}{k} \sum_{i=1}^k con_i \mathcal{L}_{SmoothL1}(j_i^{de}, j_i^{2d}) \quad (10)$$

**2D-3D Consistency Loss.** Since the outputs of the 2D branch and the 3D branch are intended to represent the same hand in different spaces, they should be consistent when they are transferred to the same domain. Through this consistency, structural information contained in the 3D reconstruction network can be introduced into the 2D keypoint estimator, and meanwhile the estimated 2D keypoints can provide joint-wise geometric cues for 3D hand reconstruction. To this end, we propose a novel 2D-3D consistency

loss to link per projected 2D joint  $j_i^{pro}$  with its corresponding estimated 2D joint  $j_i^{2d}$ :

$$E_{con} = \frac{1}{k} \sum_{i=1}^k \mathcal{L}_{SmoothL1}(j_i^{pro}, j_i^{2d}) \quad (11)$$

### 3.3 Consistent Self-supervised Hand Reconstruction from video sequences

The S<sup>2</sup>HAND(V) model learns consistent self-supervised 3D hand reconstruction from video sequences via training weight-shared S<sup>2</sup>HAND models with temporal constraints, including a quaternion loss and a T&S consistency loss.

#### 3.3.1 Quaternion loss

We reformulate hand motion in joint rotation perspective. We choose the unit quaternion [71], [72], [73], [74] as our joint rotation representation, which can represent spatial orientations and rotations of elements in a convenient and efficient way. The Unit quaternion associated with a spatial rotation is constructed as:

$$\mathbf{q} = \left( \cos \frac{\alpha}{2}, \sin \frac{\alpha}{2} \vec{\mathbf{u}} \right) \quad (12)$$

where  $\alpha$  is the rotation angle and  $\vec{\mathbf{u}}$  denotes the rotation axis in  $\mathbb{R}^3$ . Notably,  $\mathbf{q}$  can represent both rotation and orientation.

Smooth orientation transition  $\mathbf{q}_t$  between initial  $\mathbf{q}_0$  joint orientation and final  $\mathbf{q}_1$  joint orientation is defined by a unique axis  $\vec{\mathbf{v}}$  and corresponding rotation angle  $\beta$  around the axis. The transition process can be expressed as follows:

$$\mathbf{q}_t = (\mathbf{q}_1 \mathbf{q}_0^{-1})^{\phi(t)} \mathbf{q}_0 = \left( \cos \frac{\beta}{2}, \sin \frac{\beta}{2} \vec{\mathbf{v}} \right)^{\phi(t)} \mathbf{q}_0 \quad (13)$$

where  $\mathbf{q}_0^{-1}$  represents the inverse of  $\mathbf{q}_0$ , and the product operation here is the Hamilton product. The  $\phi(t)$  denotes a monotonically non-decreasing function, ranges from 0 to 1 and controls the orientation transition from  $\mathbf{q}_0$  to  $\mathbf{q}_1$ . When  $\phi(t)$  equals 0 and 1,  $\mathbf{q}_t$  will equals to  $\mathbf{q}_0$  and  $\mathbf{q}_1$  respectively. In order to reduce the computational cost brought by the Hamilton product, we further rewrite Eq. 13 as a linear combination of the two quaternion  $\mathbf{q}_0$  and  $\mathbf{q}_1$ :

$$\mathbf{q}_t = (\mathbf{q}_1 \mathbf{q}_0^{-1})^{\phi(t)} \mathbf{q}_0 = Norm[\mu(t) \mathbf{q}_0 + \varepsilon(t) \mathbf{q}_1] \quad (14)$$

where  $Norm[\cdot]$  denotes normalization to ensure the result is a unit quaternion.  $\mu(t)$  and  $\varepsilon(t)$  are time-dependent coefficients which are determined by  $\phi(t)$ . One instance of Eq. 14 is Slerp [73], which is a widely used linear quaternion interpolation method with constant rotation speed, assuming  $\phi(t) = t$ :

$$\mathbf{q}_t = (\mathbf{q}_1 \mathbf{q}_0^{-1})^t \mathbf{q}_0 = \frac{\sin((1-t)\theta)}{\sin \theta} \mathbf{q}_0 + \frac{\sin(t\theta)}{\sin \theta} \mathbf{q}_1 \quad (15)$$

where  $\theta$  is the included angle between  $\mathbf{q}_0$  and  $\mathbf{q}_1$  as two vectors, which can be computed by:

$$\theta = \frac{\mathbf{q}_1 \cdot \mathbf{q}_0}{\|\mathbf{q}_1\| \|\mathbf{q}_0\|} \quad (16)$$

where  $\cdot$  denotes inner product of two vectors and  $\|\cdot\|$  is the magnitude of a vector.

Instead of generating interpolated poses as psuedo-labels with one specific  $\phi(t)$  for supervision, we propose

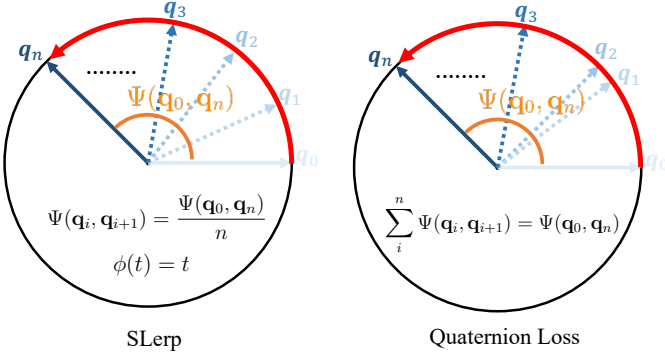


Fig. 4: Comparison between our quaternion Loss and SLerp. The circle represents a 2D projective plane of 4D unit quaternion sphere. The red arch denotes the set of quaternion that satisfies Eq. 13, which ensures smooth orientation transition. The equation in each circle represents the corresponding prior. The remaining symbols can be found in Section 3.3. As can be seen, both SLerp and quaternion loss has the prior to make sure Eq. 13 is satisfied. However SLerp has an additional prior  $\phi(t) = t$ , while our Quaternion loss covers all possible  $\phi(t)$ , which allows smooth orientation transition at all possible speed.

a quaternion loss function to cover all possible joint rotation speeds as following:

$$E_{quat} = \left\| \sum_{i=1}^{n-1} \Psi(H_i, H_{i+1}) - \Psi(H_1, H_n) \right\| \quad (17)$$

where  $\Psi$  is the function to compute the rotation angle  $\beta$  between two quaternion, and  $H_i$  denotes the output hand pose represented in quaternion of frame  $i$ . In practice,  $H_i$  is the concatenation of  $i$ -th pose vector  $\theta_i$  and  $i$ -th rotation  $R_i$  to cover all 21 hand joints:

$$H_i = Quaternion(Concatenate[\theta_i, R_i]) \quad (18)$$

where *Quaternion* denotes the transformation from representation of MANO outputs to quaternion representation and *Concatenate* denotes the concatenation operation. The comparison between the proposed quaternion loss and SLerp is illustrated in Fig.4.

To understand the proposed quaternion loss, there are two facts need to be clarified. One is that the quaternion interpolation is essentially finding a rotation curve through a fixed rotation axis between two poses, as suggested by Eq. 13. The other is that the rotation angle  $\beta$  in the quaternion space relates to included angle  $\theta$  in vector space, as indicated by Eq. 14. Specifically:

$$\cos \frac{\beta}{2} = \cos \theta \quad (19)$$

which provides an efficient way to compute  $\beta$  and is derived from:

$$\Re(\mathbf{q}_1 \mathbf{q}_0^{-1}) = \Re\left(\cos \frac{\beta}{2}, \sin \frac{\beta}{2} \vec{v}\right) = \|\mathbf{q}_1\| \|\mathbf{q}_0\| \cos \theta \quad (20)$$

where  $\Re$  represents the real part of a quaternion,  $\mathbf{q}_0$ ,  $\mathbf{q}_1$ ,  $\beta$  and  $\vec{v}$  are the same as before.  $\|\cdot\|$  is the magnitude of a vector.  $\theta$  denotes the included angle between  $\mathbf{q}_0$  and  $\mathbf{q}_1$  as two vectors. Eq. 20 can be deduced by comparing the inner product and the Hamilton product of the  $\mathbf{q}_0$  and  $\mathbf{q}_1$ .

### 3.3.2 T&S consistency loss

We introduce a regularization term on texture and shape to consider consistency of hand appearance in videos, and accordingly a T&S loss is formulated:

$$E_{T\&S} = \sum_{i=1}^n \|C_i - \bar{C}\| + \sum_{i=1}^n \|\beta_i - \bar{\beta}\| \quad (21)$$

where  $C_i$  and  $\beta_i$  are the  $i$ -th texture and shape of the sequential reconstruction output,  $\bar{C}_i$  and  $\bar{\beta}_i$  are the corresponding average of the sequential output. A low standard deviation of sequential hand appearance reconstruction from video sequences is promoted by this loss function.

### 3.3.3 Training Objective

Our overall training loss  $E_{S^2HAND(V)}$  consists of three parts, including a  $S^2HAND$  loss  $E_{S^2HAND}$ , a quaternion loss  $E_{quat}$  and a T&S loss  $E_{T\&S}$ :

$$E_{S^2HAND(V)} = E_{S^2HAND} + w_{quat} E_{quat} + w_{ts} E_{T\&S} \quad (22)$$

where  $E_{S^2HAND}$  is the same as that in Section 3.2.4. For  $E_{quat}$  and  $E_{T\&S}$ , please refer to Section 3.3.1 and Section 3.3.2 respectively. The constant weights  $w_{quat}$  and  $w_{ts}$  are used to balance the three terms.

## 4 EXPERIMENTS

### 4.1 Datasets

We evaluate our method on two challenging realistic datasets, both of which are aiming for assessing 3D joints and 3D meshes. The results are reported through online submission systems<sup>3,4</sup>. We also adopt another dataset to provide in-the-wild data.

The FreiHAND dataset [44] is a large-scale real-world dataset, which contains 32,560 training samples and 3,960 test samples. For each training sample, one real RGB image and extra three images with different synthetic backgrounds are provided. Part of the sample is a hand grabbing an object, but it does not provide any annotations for the foreground object, which poses additional challenges.

The HO-3D dataset [75] collects color images of a hand interacting with an object. The dataset is made of 68 sequences, totaling 77,558 frames of 10 users manipulating one among 10 different objects. The training set contains 66,034 images and the test set contains 11,524 images. The objects in this dataset are larger than that in FreiHAND, thus resulting in larger occlusions to hands. We use this dataset in two cases. In the case of self-supervised hand reconstruction from image collections with  $S^2HAND$ , we do not use the sequence information provided by HO-3D and mix all sequences as a image collection. In the case of self-supervised hand reconstruction from video sequences with  $S^2HAND(V)$ , we make use of the sequence information and compose the training batch accordingly. Details can be found in Section 4.3.

The YT 3D dataset [36] contains 116 in-the-wild videos, which is comprised of 102 train videos, 7 validation videos and 7 test videos, along with 47125, 1525 and 1525 hand

3. <https://competitions.codalab.org/competitions/21238>

4. <https://competitions.codalab.org/competitions/22485>

annotations. We only use this dataset as extra in-the-wild training data in Section 4.5.3 without any annotations. Since the 102 train videos are edited with lots of cutaway and only part of videos are accessible due to copyright issues, we preprocess this dataset by filtering out unavailable videos and discontinuous hand motion frames according to the detected 2D keypoints, yielding 34 train videos containing 21628 frames with detected 2D keypoints.

## 4.2 Evaluation Metrics

We evaluate 3D hand reconstruction by evaluating 3D joints and 3D meshes. For 3D joints, we report the **mean per joint position error** (MPJPE) in the Euclidean space for all joints on all test frames in *cm* and the **area under the curve** (AUC) of the PCK AUC<sub>J</sub>. Here, the PCK refers to the percentage of correct keypoints, is plotted using 100 equally spaced thresholds between *0mm* to *50mm*. For 3D meshes, we report the **mean per vertex position error** (MPVPE) in the Euclidean space for all joints on all test frames in *cm* and the AUC of the percentage of correct vertex AUC<sub>V</sub>. We also compare the F-score [76] which is the harmonic mean of recall and precision for a given distance threshold. We report distance threshold at *5mm* and *15mm* and report F-score of mesh vertices at *5mm* and *15mm* by  $F_5$  and  $F_{15}$ . Following the previous works [44], [75], we compare aligned prediction results with Procrustes alignment, and all 3D results are evaluated by the online evaluation system. For 2D joints, we report the MPJPE in *pixel* and the curve plot of **fraction of joints within distance**. For smooth hand reconstruction, we report the **acceleration error** (ACC-ERR) and the **acceleration**(ACC) which are first proposed in [77]. ACC-ERR measures average difference between ground truth acceleration and the acceleration of the predicted 3D joints in *mm/s<sup>2</sup>* while ACC calculates mean acceleration of the predicted 3D joints in *mm/s<sup>2</sup>*. Generally, lower ACC-ERR and ACC indicate smoother sequence predictions. For shape and texture consistency in sequence predictions, we report the **standard deviation** of the corresponding sequence outputs, in which low deviation means coherent and consistent sequence predictions.

## 4.3 Implementation Details

Pytorch [78] is used for implementation. For the 3D reconstruction network, the EfficientNet-b0 [65] is pre-trained on the ImageNet dataset. The 2D keypoint estimator along with the 2D-3D consistency loss is optionally used. If we train the whole network with the 2D keypoint estimator, a stage-wise training scheme is used. We train the 2D keypoint estimator and 3D reconstruction network by 90 epochs separately, where  $E_{3d}$  and  $E_{2d}$  are used, respectively. The initial learning rate is  $10^{-3}$  and reduced by a factor of 2 after every 30 epochs.

If we train S<sup>2</sup>HAND with image collections, we finetune the whole network with  $E$  by 60 epochs with the learning rate initialized to  $2.5 \times 10^{-4}$ , and reduced by a factor of 3 after every 20 epochs. We use Adam [79] to optimize the network weights with a batch size of 64. We train our model on two NVIDIA Tesla V100 GPUs, which takes around 36 hours for training on FreiHAND. Otherwise, training S<sup>2</sup>HAND(V) with video sequences, for a training batch,

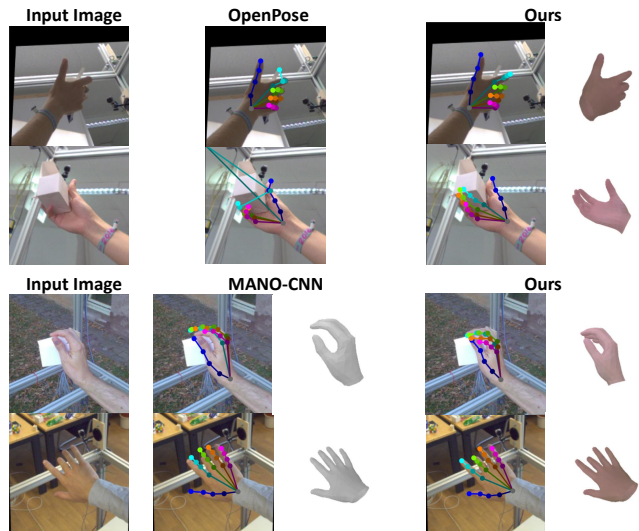


Fig. 5: Qualitative comparison to OpenPose [26] and MANO-CNN on the FreiHAND test set. For OpenPose, we visualize detected 2D keypoints. For our method and MANO-CNN, we visualize projected 2D keypoints and 3D mesh.

we first randomly sample a fixed number of sequences from training sequences, then randomly sample successive frames of fixed length in these sampled sequences, finally combine these frames to compose a batch. The learning rate, the reducing schedule, and the Adam optimizer are set the same as before.

For the weighting factors, we set  $w_{3d} = 1$ ,  $w_{2d} = 0.001$ ,  $w_{con} = 0.0002$ ,  $w_{geo} = 0.001$ ,  $w_{photo} = 0.005$ ,  $w_{quat} = 0.05$ ,  $w_{ts} = 0.01$ ,  $w_{regu} = 0.01$ ,  $w_{ori} = 100$ ,  $w_{SSIM} = 0.2$ ,  $w_C = 0.5$ ,  $w_s = 10000$  and  $w_J = 10$ .

## 4.4 Comparison with State-of-the-art Methods

We give comparison on FreiHAND with four recent model-based fully-supervised methods [24], [25], [42], [44] and a state-of-the-art weakly-supervised method [19] in Table 1. Note that [80] is not included here since it designs an advanced “image-to-lixel” prediction instead of directly regress MANO parameters. Our approach S<sup>2</sup>HAND focuses on providing a self-supervised framework with lightweight components, where the hand regression scheme is still affected by highly non-linear mapping. Therefore, we make a fairer comparison with popular model-based methods [24], [25], [42], [44] to demonstrate the performance of this self-supervised approach. Without using any annotation, our approach S<sup>2</sup>HAND outperforms [24], [44] on all evaluation metrics and achieves comparable performance to [25], [42]. [19] only outputs 3D pose, and its pose performance is slightly better than our results on FreiHAND test set but with much more training data used including RHD dataset [20] (with 40,000+ synthetic images and 3D annotations) as well as 2D ground truth annotation of the FreiHAND.

In the hand-object interaction scenario, we compare with three recent fully-supervised methods on HO-3D in Table 2. Compared to the hand branch of [24], both of our self-supervised models S<sup>2</sup>HAND and S<sup>2</sup>HAND(V) show higher mesh reconstruction performance where we get a 14% and 16% reduction in MPVPE respectively. Compared with [23], which is a fully-supervised joint hand-object pose



TABLE 1: Comparison of main results on the FreiHAND test set. The performance of our self-supervised method S<sup>2</sup>HAND is comparable to the recent fully-supervised and weakly-supervised methods. [19]\* also uses synthetic training data with 3D supervision. Note that FreiHAND is not presented with video sequences, which disables learning of S<sup>2</sup>HAND(V).

Supervision	Method	AUC <sub>J</sub> ↑	MPJPE↓	AUC <sub>V</sub> ↑	MPVPE↓	F <sub>5</sub> ↑	F <sub>15</sub> ↑
3D	[44](2019)	0.35	3.50	0.74	1.32	0.43	0.90
	[24](2019)	0.74	1.33	0.74	1.33	0.43	0.91
	[42](2019)	<b>0.78</b>	<b>1.10</b>	<b>0.78</b>	<b>1.09</b>	<b>0.52</b>	<b>0.93</b>
	[25](2020)	<b>0.78</b>	<u>1.11</u>	<b>0.78</b>	<u>1.10</u>	<u>0.51</u>	<b>0.93</b>
2D	[19](2020)*	<b>0.78</b>	1.13	-	-	-	-
-	S <sup>2</sup> HAND	<u>0.77</u>	1.18	<u>0.77</u>	1.19	0.48	<u>0.92</u>

TABLE 2: Comparison of main results on the HO-3D test set. Without using any object information and hand annotation, our S<sup>2</sup>HAND model performs comparably with recent fully-supervised methods [23]. With further temporal constraints, our S<sup>2</sup>HAND(V) even surpass [23]

Supervision	Method	AUC <sub>J</sub> ↑	MPJPE↓	AUC <sub>V</sub> ↑	MPVPE↓	F <sub>5</sub> ↑	F <sub>15</sub> ↑
3D	[24](2019)	-	-	-	1.30	0.42	0.90
	[75](2020)	-	-	-	<b>1.06</b>	<b>0.51</b>	<b>0.94</b>
	[23](2020)	<u>0.773</u>	<u>1.11</u>	0.773	1.14	0.43	<u>0.93</u>
-	S <sup>2</sup> HAND	<u>0.773</u>	1.14	<u>0.777</u>	1.12	0.45	<u>0.93</u>
-	S <sup>2</sup> HAND(V)	<b>0.780</b>	<b>1.10</b>	<b>0.782</b>	<u>1.09</u>	<u>0.46</u>	<b>0.94</b>

TABLE 3: Ablation studies for different losses used in our method on the FreiHAND testing set. Refer to Section 4.5.1 for details.

Losses					MPJPE↓	MPVPE↓	AUC <sub>J</sub> ↑	AUC <sub>V</sub> ↑	F <sub>5</sub> ↑	F <sub>15</sub> ↑
$E_{loc}$	$E_{regu}$	$E_{ori}$	$E_{2d}$ , $E_{con}$	$E_{photo}$						
✓					1.54	1.58	0.696	0.687	0.387	0.852
✓		✓			1.24	1.26	0.754	0.750	0.457	0.903
✓		✓	✓		1.19	1.20	0.764	0.763	0.479	0.915
✓		✓	✓	✓	<b>1.18</b>	<b>1.19</b>	<b>0.766</b>	<b>0.765</b>	<b>0.483</b>	<b>0.917</b>

estimation method, our S<sup>2</sup>HAND obtains comparable joints and shape estimation results, while our S<sup>2</sup>HAND(V) even surpass [23]. [75] gets slightly better shape estimation results than ours, which may be due to it uses multi-frame joint hand-object pose refinement and mesh supervision.

In Fig. 5, we show 2D keypoint detection from OpenPose [26] and our S<sup>2</sup>HAND results of difficult samples. We also compare the reconstruction results with MANO-CNN, which directly estimates MANO parameters with a CNN [44], but we modify its backbone to be the same as ours. Our results are more accurate and additionally with texture.

#### 4.5 Self-comparison

In Section 4.5.1 and Section 4.5.2, we conduct extensive self-comparisons to verify the effectiveness of each component of our models S<sup>2</sup>HAND and S<sup>2</sup>HAND(V). In Section 4.5.3, we explore the effect of absorbing extra in-the-wild video sequences with S<sup>2</sup>HAND(V).

##### 4.5.1 Hand reconstruction from image collection

For self-supervised hand reconstruction from image collection with S<sup>2</sup>HAND, we conduct ablation studies on FreiHAND, since it is a widely used challenging dataset for hand pose and shape estimation from single RGB images.

First, we give evaluation results on FreiHAND of settings with different components along with corresponding loss terms used in the network in Table 3. The baseline only uses the 3D branch with  $E_{loc}$  and  $E_{regu}$ , then we add  $E_{ori}$  which helps the MPJPE and MPVPE decrease by 19.5%. After adding the 2D branch with  $E_{2d}$  and the 2D-3D consistency constrain  $E_{con}$ , the MPJPE and MPVPE further

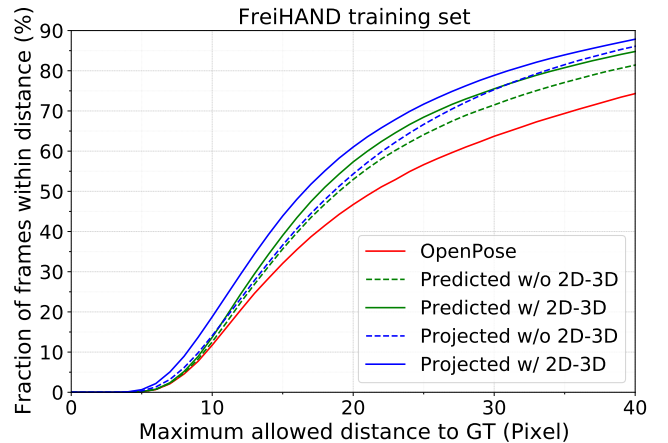


Fig. 6: A comparison of 2D keypoint sets used or outputted at the training stage on FreiHAND. The fraction of frames within maximum joint distance is plotted. Refer to Section 4.5.1 for details.

reduce by 4%. The  $E_{photo}$  slightly improves the pose and shape estimation results.

Then, we make comparison of different 2D keypoint sets. In our approach, there are three sets of 2D keypoints, including detected keypoints  $J^{de}$ , estimated 2D keypoints  $J^{2d}$ , and output projected keypoints  $J^{pro}$ , where  $J^{de}$  is used as supervision terms while  $J^{2d}$  and  $J^{pro}$  are output items. In our setting, we use multiple 2D representations to boost the final 3D hand reconstruction, so we do not advocate the novelty of 2D hand estimation, but compare 2D accuracy in the training set to demonstrate the effect of learning from noisy supervision and the benefits of the proposed 2D-3D consistency. Although we use OpenPose

TABLE 4: Comparison of accuracy performance of different motion-related constraints on the HO-3D test set. Quaternion loss shows its effectiveness over similar loss functions modeling smoothness. T&S consistency loss witnesses a further improvement in  $AUC_J$  and  $AUC_V$ .

Method	$AUC_J\uparrow$	MPJPE $\downarrow$	$AUC_V\uparrow$	MPVPE $\downarrow$	$F_5\uparrow$	$F_{15}\uparrow$
S <sup>2</sup> HAND	0.773	1.14	0.777	1.12	0.45	0.93
S <sup>2</sup> HAND(V) (w/ Temporal Loss [60])	0.771	1.15	0.773	1.14	0.44	0.93
S <sup>2</sup> HAND(V) (w/ Smooth Loss [32])	0.774	1.13	0.776	1.12	0.45	0.93
S <sup>2</sup> HAND(V) (w/ Quaternion Loss)	0.779	<b>1.10</b>	0.781	<b>1.09</b>	0.46	0.94
S <sup>2</sup> HAND(V) (w/ Quaternion Loss, T&S Loss)	<b>0.780</b>	<b>1.10</b>	<b>0.782</b>	<b>1.09</b>	<b>0.46</b>	<b>0.94</b>

TABLE 5: Comparison of smoothness performance of different motion-related constraints on the HO-3D test set. Quaternion loss gives the smoothest predictions and is highly in line with ACC and ACC-ERR.

Method	Train set			Test set	
	ACC-ERR $\downarrow$	ACC $\downarrow$	Quaternion Loss $\downarrow$	ACC $\downarrow$	Quaternion Loss $\downarrow$
S <sup>2</sup> HAND	2.85	2.29	0.014	3.68	0.020
S <sup>2</sup> HAND(V) (w/ Temporal Loss [60])	2.57	1.96	0.011	2.87	0.015
S <sup>2</sup> HAND(V) (w/ Smooth Loss [32])	2.89	2.29	0.014	2.89	0.015
S <sup>2</sup> HAND(V) (w/ Quaternion Loss)	<b>2.23</b>	<b>1.59</b>	<b>0.008</b>	<b>2.81</b>	<b>0.014</b>

outputs as the keypoint supervision source (see *OpenPose* in Fig. 6), we get lower overall 2D MPJPE when we pre-train the 2D and 3D branches separately (see *Predicted w/o 2D-3D* and *Projected w/o 2D-3D* in Fig. 6). After finetuning these two branches with 2D-3D consistency, we find both of them gain additional benefits. After the finetuning, the 2D branch (*Predicted w/ 2D-3D*) gains 5.4% reduction in 2D MPJPE and the 3D branch (*Projected w/ 2D-3D*) gains 9.3% reduction in 2D MPJPE. From the curves, we can see that 2D keypoint estimation (including OpenPose and our 2D branch) gets higher accuracy in small distance thresholds while the regression-based methods (*Projected w/o 2D-3D*) get higher accuracy with larger distance threshold. From the curves, the proposed 2D-3D consistency can improve the 3D branch in all distance thresholds, which verifies the rationality of our network design.

Last, we compare the weak-supervised (WSL) scheme using ground truth annotations with our self-supervised (SSL) approach to investigate the ability of our method to handle noisy supervision sources. Both settings use the same network structure and implementation, and WSL uses the ground truth 2D keypoint annotations whose keypoint confidences are set to be the same. As shown in Table 6, our SSL

TABLE 6: Comparison of self-supervised results and weakly-supervised results. Refer to Section 4.5.1 for details.

Dataset	Method	$AUC_J\uparrow$	$AUC_V\uparrow$	$F_5\uparrow$	$F_{15}\uparrow$
FreiHAND	WSL	0.730	0.725	0.42	0.89
	SSL	<b>0.766</b>	<b>0.765</b>	<b>0.48</b>	<b>0.92</b>
HO-3D	WSL	0.765	0.769	0.44	<b>0.93</b>
	SSL	<b>0.773</b>	<b>0.777</b>	<b>0.45</b>	<b>0.93</b>

approach has better performance than WSL settings on both datasets. We think this is because the detection confidence information is embedded into the proposed loss functions, which helps the network discriminate different accuracy in the noisy samples. In addition, we find that the SSL method outperforms the WSL method in a smaller amplitude on HO-3D (by 1.0%) than that on FreiHand (by 4.9%). We think this is because the HO-3D contains more occluded hands, resulting in poor 2D detection results. Therefore, we conclude that noisy 2D keypoints can supervise shape

learning for the hand reconstruction task, while the quality of the unlabeled image also has a certain impact.

#### 4.5.2 Consistent Hand reconstruction from video sequences

For consistent self-supervised hand reconstruction from video sequences with S<sup>2</sup>HAND(V), we conduct ablation studies on HO3D since it is a widely used challenging dataset that presents hand-object interaction images with sequence information.

We first study the accuracy performance of quaternion loss in comparison with other commonly used motion-related constraints modeling smoothness in sequence outputs. The compared constraints include temporal loss from [32] closing neighboring poses as much as possible and smooth loss from [60] limiting neighboring pose variation with a threshold. Quantitative and Qualitative results are presented in Table 4 and Fig. 7.

Compared to S<sup>2</sup>HAND, S<sup>2</sup>HAND(V) with quaternion loss improves single frame prediction by reducing 3.5% in MPVPE, while S<sup>2</sup>HAND(V) with smooth loss from [32] only gets a reduction of less than 1% in MPVPE and S<sup>2</sup>HAND(V) with temporal loss from [60] even degenerates the accuracy. We think this is because weak supervision is prone to optimize models in the wrong direction and suffers from being too sketchy and limited under self-supervised settings. The temporal loss from [60] is beneficial when the 3D annotation is available but may collapse the model by making the network insensitive to the high-frequency details in absence of strong supervision signals. The smooth loss from [32] introduces threshold, but in exchange enlarges the solution space and vanishes when the threshold is exceeded. In contrast, quaternion loss narrows the solution space based on hand structures and hand motion dynamics and provides more significant supervision signals, which proves its effectiveness over other similar constraints in accuracy.

We next explore our quaternion loss with different configurations in terms of the actual frame interval (interv) of sampled frames and the frame number (See  $n$  in Eq. 17). The results are shown in Table 7. The medium interv achieves the best performance. We attribute this to two reasons. On one hand, large interv may witness changes of the joint rota-

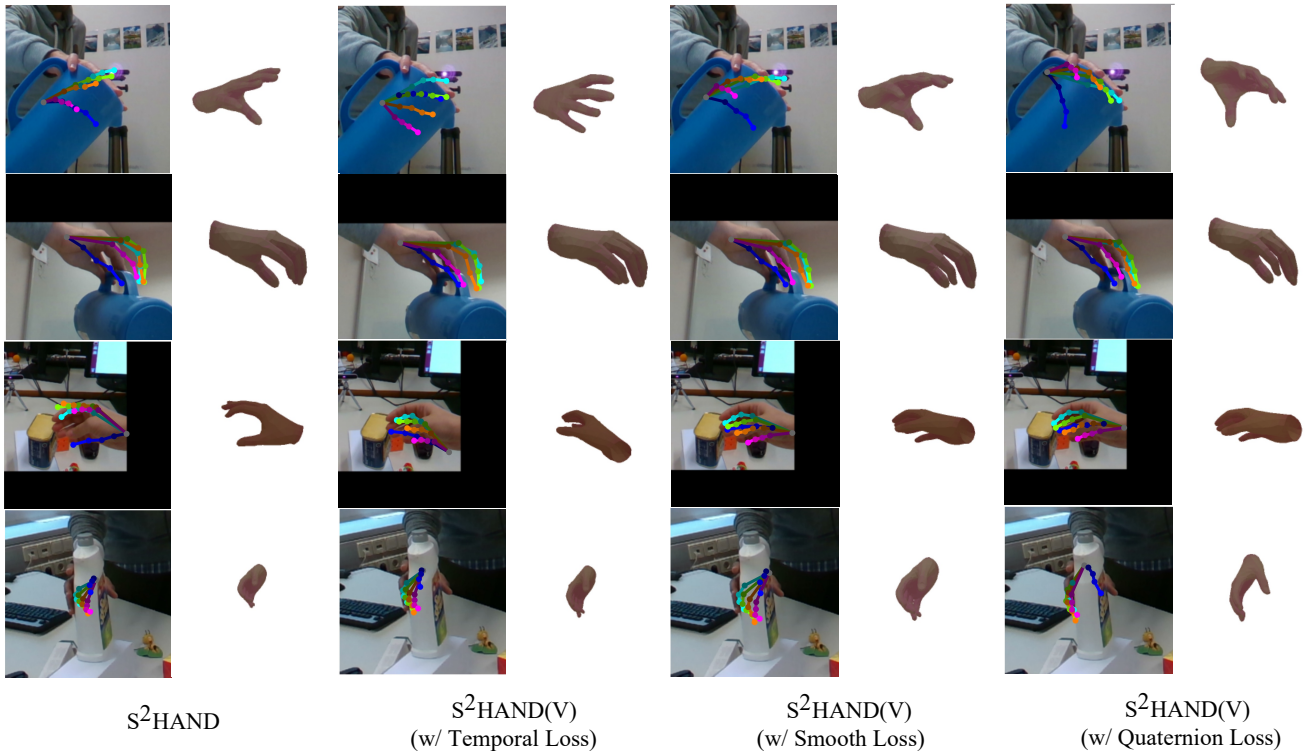


Fig. 7: Qualitative comparison of different motion-related constraints on the HO-3D test set. Our  $S^2\text{HAND}(V)$  with quaternion loss achieves best qualitative results.

TABLE 7: Comparison of different configurations of quaternion loss on the HO-3D test set.

Config	AUC <sub>J</sub> ↑	MPJPE↓	AUC <sub>V</sub> ↑	MPVPE↓
interv=1, n=3	0.778	1.11	0.780	1.10
interv=3, n=3	<b>0.780</b>	<b>1.10</b>	<b>0.782</b>	<b>1.09</b>
interv=6, n=3	0.775	1.13	0.776	1.12
interv=3, n=6	0.774	1.13	0.777	1.12

tion axis in sampled frames, which contradicts the fixed axis prior in quaternion interpolation (See Section 3.3.1). On the other hand, small interv only witnesses small rotation angles, which limits the effect of quaternion loss. In addition, increasing n causes model accuracy to drop. We believe this is because optimizing multiple unconfident predictions at the same time puts an extra burden on the gradient-descent-based optimizer and unstabilizes the learning procedure. From above, we conclude that the best configuration of quaternion loss depends on the frame rates of input video sequences and the confidence of the output. Adjusting the configuration of quaternion loss dynamically according to the input and the output can be a promising direction for future work.

We then compare smoothness performance of quaternion loss with others by concatenate their single frame predictions to corresponding sequences predictions. The results are reported on both train set and test set in Table 5. Note that we only report ACC-ERR on train set since 3D ground truth is required to calculate ACC-ERR. As shown in Table 5, all smoothness related prior improve the smoothness of the sequence outputs, and our proposed quaternion loss achieves the best performance in all evaluation matrices. [60] comes second in terms of smoothness, but shows the

worst performance on accuracy in Table 4. We think better smoothness does not imply higher accuracy, where a trade-off between smoothness and accuracy is shown in some cases. Our quaternion loss differently does best on both accuracy and smoothness, which again proves its superiority over similar methods.

In addition, we report the average quaternion loss of the concatenated sequences predictions. We find that our quaternion loss is highly in line with ACC and ACC-ERR, which is encouraging since they are calculated from completely different angles. ACC-ERR and ACC regard no hand structure and hand motion characteristic, rely solely on mechanics in terms of acceleration, while quaternion loss does the opposite. Thus, we think our proposed quaternion loss not only proves its advantages over other loss functions in smoothness, but is capable of being the metric measuring smoothness of sequence predictions as well.

We last inspect the effect of regularizing outputs of hand shape and texture in sequence predictions with T&S Consistency loss. The results are in Table 4 and Table 9. We observe a certain amount of improvement in both consistency and accuracy by further adding T&S consistency loss. However, the enhancement is insignificant, specifically only leading to an increase of 0.001 in AUC<sub>J</sub>, AUC<sub>V</sub> and a decrease of 0.001 in shape standard deviation. We contribute this to three possible reasons. First, HO3D contains lots of occlusions from interacting objects, causing incoherent hand shape and texture inference. Second, We already have shape and texture regularization terms in Section 3.2.4, weakening the effect of T&S Consistency. Third, simply adding a consistency regularization term in loss function can not provide strong enough self-supervision signals. Additionally, we find that

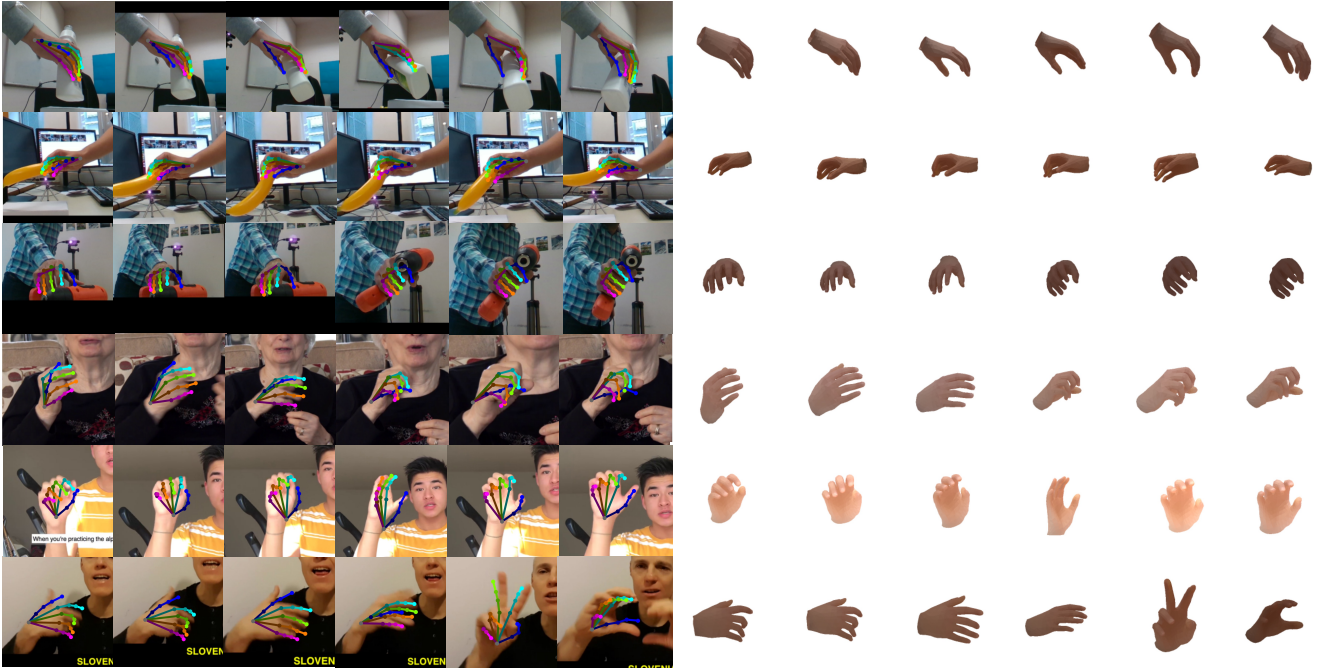


Fig. 8: Qualitative results of  $S^2\text{HAND}(V)$  with extra in-the-wild data. The first three rows show results from HO3D and the last three rows show results from YT 3D.

TABLE 8: Results of absorbing extra in-the-wild data from YT 3D on the HO3D test set. \* represents changing camera model from perspective to orthogonal model, which enables learning with in-the-wild data without camera information.

Method	AUC <sub>J</sub> ↑	MPJPE↓	AUC <sub>V</sub> ↑	MPVPE↓	F <sub>5</sub> ↑	F <sub>15</sub> ↑
$S^2\text{HAND}$	0.773	1.14	0.777	1.12	0.45	0.93
$S^2\text{HAND}^*$	0.770	1.15	0.774	1.13	0.45	0.93
$S^2\text{HAND}(V)^*$ (w/ Quaternion Loss)	0.778	1.11	0.780	1.10	0.45	<b>0.94</b>
$S^2\text{HAND}(V)^*$ (w/ Quaternion Loss) + YT 3D data	<b>0.782</b>	<b>1.09</b>	<b>0.783</b>	<b>1.09</b>	<b>0.46</b>	<b>0.94</b>

TABLE 9: Results of hand appearance consistency of our methods on the HO-3D test set.

Method	Texture S.D.	Shape S.D.
$S^2\text{HAND}$	0.12	0.042
$S^2\text{HAND}(V)$ (w/ Quaternion Loss)	<b>0.11</b>	0.035
$S^2\text{HAND}(V)$ (w/ Quaternion Loss, T&S Loss)	<b>0.11</b>	<b>0.034</b>

our quaternion loss decreases shape standard a lot and achieves comparable results as adding T&S consistency loss further. We think this is because accurate pose estimations can be beneficial to shape predictions, which proves the superiority of our method again. In conclusion, we believe that shape and texture consistency can help improve the prediction performance, but has limited effects, and pose accuracy also do help to shape and texture consistency.

#### 4.5.3 Hand reconstruction with extra in-the-wild data

For Hand reconstruction with extra in-the-wild data to fully exploit the advantage of our self-supervised method  $S^2\text{HAND}(V)$ , we use 34 train videos from YT 3D [36] and switch to orthogonal camera model with corresponding camera projection to enable learning with in-the-wild data without camera information.

The results are presented in Table 8 and Fig. 8. Changing the camera model makes the model performance drop a little, which may be caused by the ambiguity of camera focal length. Then, imposing proposed quaternion loss boosts

the performance by 3.4%, which conforms to experiments results in Section 4.5.2. Finally, adding extra in-the-wild data further improves our model by 1.8%, resulting in 1.09cm in MPVPE, which is the best result we can get on the HO-3D test set. From above, we see that our proposed method is able to utilize extra in-the-wild data without any camera information and benefits from these training data. It is worth noticing that there is a certain domain gap between HO-3D and YT 3D since HO-3D regards hand-object interaction scenario while YT 3D is mostly comprised of sign language videos. However, the improvement on HO-3D has still been witnessed, which we think proves the significance of utilizing in the data and the advantage of the proposed method.

## 5 CONCLUSION

We have presented self-supervised 3D hand reconstruction models  $S^2\text{HAND}$  and  $S^2\text{HAND}(V)$  which can be trained from a collection of hand images and video sequences without manual annotations, respectively. The 3D hand reconstruction network in both models encodes the input image into a set of meaningful semantic parameters that represent hand pose, shape, texture, illumination, and the camera viewpoint. These parameters can be decoded into a textured 3D hand mesh as well as a set of 3D joints, and in turn, 3D mesh and joints can be projected into the 2D image space, which enables our network to be

end-to-end learned. We further exploit the self-supervision signals embedded in hand motion videos through a novel quaternion loss works on hand pose and a regularization term conducts on hand appearance, resulting in obtaining more consistent hand reconstruction. Experimental results show that our models perform well under noisy supervision sources captured from 2D hand keypoint detection, and achieve comparable performance to the state-of-the-art fully-supervised method with the usage of motion-related information. Moreover, the experimenting on in-the-wild video data shows that our self-supervised model is effective to learn useful information from in-the-wild data to further improve its performance.

## ACKNOWLEDGMENT

## REFERENCES

- [1] H. Lee, M. Billinghurst, and W. Woo, "Two-handed tangible interaction techniques for composing augmented blocks," *Virtual Reality*, vol. 15, no. 2-3, pp. 133-146, 2011.
- [2] N. C. Camgoz, S. Hadfield, O. Koller, H. Ney, and R. Bowden, "Neural sign language translation," in *Conference on Computer Vision and Pattern Recognition*, 2018, pp. 7784-7793.
- [3] N. C. Camgoz, O. Koller, S. Hadfield, and R. Bowden, "Sign language transformers: Joint end-to-end sign language recognition and translation," in *Conference on Computer Vision and Pattern Recognition*, 2020, pp. 10023-10033.
- [4] M. Höll, M. Oberweger, C. Arth, and V. Lepetit, "Efficient physics-based implementation for realistic hand-object interaction in virtual reality," in *Conference on Virtual Reality and 3D User Interfaces*, 2018.
- [5] M. Parelli, K. Papatimitriou, G. Potamianos, G. Pavlakos, and P. Maragos, "Exploiting 3d hand pose estimation in deep learning-based sign language recognition from rgb videos," in *European Conference on Computer Vision*. Springer, 2020.
- [6] Z. Tu, H. Li, D. Zhang, J. Dauwels, B. Li, and J. Yuan, "Action-stage emphasized spatiotemporal vlad for video action recognition," *IEEE Transactions on Image Processing*, vol. 28, no. 6, pp. 2799-2812, 2019.
- [7] L. Ge, H. Liang, J. Yuan, and D. Thalmann, "Robust 3d hand pose estimation from single depth images using multi-view cnns," *IEEE Transactions on Image Processing*, vol. 27, no. 9, pp. 4422-4436, 2018.
- [8] Z. Yu, J. S. Yoon, I. K. Lee, P. Venkatesh, J. Park, J. Yu, and H. S. Park, "Humbi: A large multiview dataset of human body expressions," in *Conference on Computer Vision and Pattern Recognition*, 2020, pp. 2990-3000.
- [9] Z. Zhao, T. Wang, S. Xia, and Y. Wang, "Hand-3d-studio: A new multi-view system for 3d hand reconstruction," in *IEEE International Conference on Acoustics, Speech, and Signal Processing*. IEEE, 2020, pp. 2478-2482.
- [10] G. Poier, D. Schinagl, and H. Bischof, "Learning pose specific representations by predicting different views," in *Conference on Computer Vision and Pattern Recognition*, 2018, pp. 60-69.
- [11] A. Armagan, G. Garcia-Hernando, S. Baek, S. Hampali, M. Rad, Z. Zhang, S. Xie, M. Chen, B. Zhang, F. Xiong et al., "Measuring generalisation to unseen viewpoints, articulations, shapes and objects for 3d hand pose estimation under hand-object interaction," in *European Conference on Computer Vision*, 2020.
- [12] Y. Chen, Z. Tu, L. Ge, D. Zhang, R. Chen, and J. Yuan, "So-handnet: Self-organizing network for 3d hand pose estimation with semi-supervised learning," in *International Conference on Computer Vision*, 2019.
- [13] L. Ge, H. Liang, J. Yuan, and D. Thalmann, "Robust 3d hand pose estimation in single depth images: from single-view cnn to multi-view cnns," in *Conference on Computer Vision and Pattern Recognition*, 2016.
- [14] L. Huang, J. Tan, J. Liu, and J. Yuan, "Hand-transformer: Non-autoregressive structured modeling for 3d hand pose estimation," in *European Conference on Computer Vision*, 2020.
- [15] S. Yuan, G. Garcia-Hernando, B. Stenger, G. Moon, J. Yong Chang, K. Mu Lee, P. Molchanov, J. Kautz, S. Honari, L. Ge et al., "Depth-based 3d hand pose estimation: From current achievements to future goals," in *Conference on Computer Vision and Pattern Recognition*, 2018.
- [16] V. Athitsos and S. Sclaroff, "Estimating 3d hand pose from a cluttered image," in *Conference on Computer Vision and Pattern Recognition*, 2003.
- [17] Y. Cai, L. Ge, J. Cai, and J. Yuan, "Weakly-supervised 3d hand pose estimation from monocular rgb images," in *European Conference on Computer Vision*, 2018.
- [18] U. Iqbal, P. Molchanov, T. Breuel Juergen Gall, and J. Kautz, "Hand pose estimation via latent 2.5 d heatmap regression," in *European Conference on Computer Vision*, 2018.
- [19] A. Spurr, U. Iqbal, P. Molchanov, O. Hilliges, and J. Kautz, "Weakly supervised 3d hand pose estimation via biomechanical constraints," in *European Conference on Computer Vision*, 2020.
- [20] C. Zimmermann and T. Brox, "Learning to estimate 3d hand pose from single rgb images," in *International Conference on Computer Vision*, 2017.
- [21] L. Ge, Z. Ren, Y. Li, Z. Xue, Y. Wang, J. Cai, and J. Yuan, "3d hand shape and pose estimation from a single rgb image," in *Conference on Computer Vision and Pattern Recognition*, 2019.
- [22] D. Kulon, R. A. Guler, I. Kokkinos, M. M. Bronstein, and S. Zafeiriou, "Weakly-supervised mesh-convolutional hand reconstruction in the wild," in *Conference on Computer Vision and Pattern Recognition*, 2020.
- [23] Y. Hasson, B. Tekin, F. Bogo, I. Laptev, M. Pollefeys, and C. Schmid, "Leveraging photometric consistency over time for sparsely supervised hand-object reconstruction," in *Conference on Computer Vision and Pattern Recognition*, 2020.
- [24] Y. Hasson, G. Varol, D. Tzionas, I. Kalevatykh, M. J. Black, I. Laptev, and C. Schmid, "Learning joint reconstruction of hands and manipulated objects," in *Conference on Computer Vision and Pattern Recognition*, 2019.
- [25] N. Qian, J. Wang, F. Mueller, F. Bernard, V. Golyanik, and C. Theobalt, "Parametric hand texture model for 3d hand reconstruction and personalization," in *European Conference on Computer Vision*. Springer, 2020.
- [26] Z. Cao, T. Simon, S.-E. Wei, and Y. Sheikh, "Openpose: Realtime multi-person 2d pose estimation using part affinity fields." *IEEE Transactions on Pattern Analysis and Machine Intelligence*, 2019.
- [27] Y. Chen, Z. Tu, D. Kang, L. Bao, Y. Zhang, X. Zhe, R. Chen, and J. Yuan, "Model-based 3d hand reconstruction via self-supervised learning," in *Conference on Computer Vision and Pattern Recognition*, 2021, pp. 10451-10460.
- [28] Y. Cai, L. Ge, J. Cai, N. Magnenat-Thalmann, and J. Yuan, "3d hand pose estimation using synthetic data and weakly labeled rgb images," *IEEE Transactions on Pattern Analysis and Machine Intelligence*, 2020.
- [29] L. Yang and A. Yao, "Disentangling latent hands for image synthesis and pose estimation," in *Conference on Computer Vision and Pattern Recognition*, 2019, pp. 9877-9886.
- [30] K. Lin, L. Wang, and Z. Liu, "End-to-end human pose and mesh reconstruction with transformers," in *Conference on Computer Vision and Pattern Recognition*, 2021, pp. 1954-1963.
- [31] P. Chen, Y. Chen, D. Yang, F. Wu, Q. Li, Q. Xia, and Y. Tan, "I2uv-handnet: Image-to-uv prediction network for accurate and high-fidelity 3d hand mesh modeling," in *International Conference on Computer Vision*, 2021, pp. 12929-12938.
- [32] S. Liu, H. Jiang, J. Xu, S. Liu, and X. Wang, "Semi-supervised 3d hand-object poses estimation with interactions in time," in *Conference on Computer Vision and Pattern Recognition*, 2021, pp. 14687-14697.
- [33] Y. Zhou, M. Habermann, I. Habibie, A. Tewari, C. Theobalt, and F. Xu, "Monocular real-time full body capture with inter-part correlations," in *Conference on Computer Vision and Pattern Recognition*, 2021, pp. 4811-4822.
- [34] X. Chen, Y. Liu, C. Ma, J. Chang, H. Wang, T. Chen, X. Guo, P. Wan, and W. Zheng, "Camera-space hand mesh recovery via semantic aggregation and adaptive 2d-1d registration," in *Conference on Computer Vision and Pattern Recognition*, 2021, pp. 13274-13283.
- [35] Z. Cao, I. Radosavovic, A. Kanazawa, and J. Malik, "Reconstructing hand-object interactions in the wild," in *International Conference on Computer Vision*, October 2021, pp. 12417-12426.
- [36] D. Kulon, R. A. Guler, I. Kokkinos, M. M. Bronstein, and S. Zafeiriou, "Weakly-supervised mesh-convolutional hand recon-

- struction in the wild,” in *Conference on Computer Vision and Pattern Recognition*, 2020, pp. 4990–5000.
- [37] I. Lim, A. Dielen, M. Campen, and L. Kobbelt, “A simple approach to intrinsic correspondence learning on unstructured 3d meshes,” in *European Conference on Computer Vision*, 2018, pp. 0–0.
- [38] D. Kulon, H. Wang, R. A. Güler, M. M. Bronstein, and S. Zafeiriou, “Single image 3d hand reconstruction with mesh convolutions,” in *British Machine Vision Conference*, 2019.
- [39] M. Defferrard, X. Bresson, and P. Vandergheynst, “Convolutional neural networks on graphs with fast localized spectral filtering,” *Advances in neural information processing systems*, vol. 29, pp. 3844–3852, 2016.
- [40] L. Ge, Z. Ren, Y. Li, Z. Xue, Y. Wang, J. Cai, and J. Yuan, “3d hand shape and pose estimation from a single rgb image,” in *Conference on Computer Vision and Pattern Recognition*, 2019, pp. 10 833–10 842.
- [41] J. Romero, D. Tzionas, and M. J. Black, “Embodied hands: Modeling and capturing hands and bodies together,” *ACM Transactions on Graphics*, 2017.
- [42] A. Boukhayma, R. d. Bem, and P. H. Torr, “3d hand shape and pose from images in the wild,” in *Conference on Computer Vision and Pattern Recognition*, 2019, pp. 10 843–10 852.
- [43] Y. Chen, Z. Tu, D. Kang, R. Chen, L. Bao, Z. Zhang, and J. Yuan, “Joint hand-object 3d reconstruction from a single image with cross-branch feature fusion,” *IEEE Transactions on Image Processing*, 2020.
- [44] C. Zimmermann, D. Ceylan, J. Yang, B. Russell, M. Argus, and T. Brox, “Freihand: A dataset for markerless capture of hand pose and shape from single rgb images,” in *International Conference on Computer Vision*, 2019.
- [45] S. Baek, K. I. Kim, and T.-K. Kim, “Pushing the envelope for rgb-based dense 3d hand pose estimation via neural rendering,” in *Conference on Computer Vision and Pattern Recognition*, 2019.
- [46] —, “Weakly-supervised domain adaptation via gan and mesh model for estimating 3d hand poses interacting objects,” in *Conference on Computer Vision and Pattern Recognition*, 2020, pp. 6121–6131.
- [47] J. Wang, F. Mueller, F. Bernard, S. Sorli, O. Sotnychenko, N. Qian, M. A. Otaduy, D. Casas, and C. Theobalt, “RGB2Hands: Real-Time Tracking of 3D Hand Interactions from Monocular RGB Video,” *ACM Transactions on Graphics (Proceedings of SIGGRAPH Asia)*, 2020.
- [48] Y. Zhou, M. Habermann, W. Xu, I. Habibie, C. Theobalt, and F. Xu, “Monocular real-time hand shape and motion capture using multi-modal data,” in *Conference on Computer Vision and Pattern Recognition*, 2020.
- [49] P. Panteleris, I. Oikonomidis, and A. Argyros, “Using a single rgb frame for real time 3d hand pose estimation in the wild,” in *Winter Conference on Applications of Computer Vision*, 2018.
- [50] S. Wu, C. Rupprecht, and A. Vedaldi, “Unsupervised learning of probably symmetric deformable 3d objects from images in the wild,” in *Conference on Computer Vision and Pattern Recognition*, 2020.
- [51] S. Goel, A. Kanazawa, and J. Malik, “Shape and viewpoint without keypoints,” in *European Conference on Computer Vision*, 2020.
- [52] C. Wan, T. Probst, L. V. Gool, and A. Yao, “Self-supervised 3d hand pose estimation through training by fitting,” in *Conference on Computer Vision and Pattern Recognition*, 2019.
- [53] Y. Chen, F. Wu, Z. Wang, Y. Song, Y. Ling, and L. Bao, “Self-supervised learning of detailed 3d face reconstruction,” *IEEE Transactions on Image Processing*, vol. 29, pp. 8696–8705, 2020.
- [54] A. Tewari, M. Zollhöfer, P. Garrido, F. Bernard, H. Kim, P. Pérez, and C. Theobalt, “Self-supervised multi-level face model learning for monocular reconstruction at over 250 hz,” in *Conference on Computer Vision and Pattern Recognition*, 2018.
- [55] A. Tewari, M. Zollhofer, H. Kim, P. Garrido, F. Bernard, P. Perez, and C. Theobalt, “Mofa: Model-based deep convolutional face autoencoder for unsupervised monocular reconstruction,” in *International Conference on Computer Vision Workshops*, 2017.
- [56] V. Blanz and T. Vetter, “A morphable model for the synthesis of 3d faces,” in *ACM Transactions on Graphics (Proceedings of SIGGRAPH)*, 1999, pp. 187–194.
- [57] M. de La Gorce, D. J. Fleet, and N. Paragios, “Model-based 3d hand pose estimation from monocular video,” *IEEE Transactions on Pattern Analysis and Machine Intelligence*, 2011.
- [58] M. de La Gorce, N. Paragios, and D. J. Fleet, “Model-based hand tracking with texture, shading and self-occlusions,” in *Conference on Computer Vision and Pattern Recognition*, 2008.
- [59] Y. Cai, L. Ge, J. Liu, J. Cai, T.-J. Cham, J. Yuan, and N. M. Thalmann, “Exploiting spatial-temporal relationships for 3d pose estimation via graph convolutional networks,” in *International Conference on Computer Vision*, 2019, pp. 2272–2281.
- [60] J. Yang, H. J. Chang, S. Lee, and N. Kwak, “Seqhand: Rgb-sequence-based 3d hand pose and shape estimation,” in *European Conference on Computer Vision*. Springer, 2020, pp. 122–139.
- [61] K. Fragkiadaki, S. Levine, P. Felsen, and J. Malik, “Recurrent network models for human dynamics,” in *International Conference on Computer Vision*, 2015, pp. 4346–4354.
- [62] J. Martinez, M. J. Black, and J. Romero, “On human motion prediction using recurrent neural networks,” in *Conference on Computer Vision and Pattern Recognition*, 2017, pp. 2891–2900.
- [63] E. Aksan, M. Kaufmann, and O. Hilliges, “Structured prediction helps 3d human motion modelling,” in *International Conference on Computer Vision*, 2019, pp. 7144–7153.
- [64] A. Hernandez, J. Gall, and F. Moreno-Noguer, “Human motion prediction via spatio-temporal inpainting,” in *International Conference on Computer Vision*, 2019, pp. 7134–7143.
- [65] M. Tan and Q. V. Le, “Efficientnet: Rethinking model scaling for convolutional neural networks,” in *International Conference on Machine Learning*, 2019.
- [66] H. Kato, Y. Ushiku, and T. Harada, “Neural 3d mesh renderer,” in *Conference on Computer Vision and Pattern Recognition*, 2018.
- [67] A. Newell, K. Yang, and J. Deng, “Stacked hourglass networks for human pose estimation,” in *European Conference on Computer Vision*, 2016.
- [68] X. Sun, B. Xiao, F. Wei, S. Liang, and Y. Wei, “Integral human pose regression,” in *European Conference on Computer Vision*, 2018.
- [69] P. J. Huber, “Robust estimation of a location parameter,” in *Breakthroughs in statistics*. Springer, 1992, pp. 492–518.
- [70] Z. Wang, A. C. Bovik, H. R. Sheikh, and E. P. Simoncelli, “Image quality assessment: from error visibility to structural similarity,” *IEEE Transactions on Image Processing*, 2004.
- [71] D. Pavlo, C. Feichtenhofer, M. Auli, and D. Grangier, “Modeling human motion with quaternion-based neural networks,” *International Journal of Computer Vision*, vol. 128, no. 4, pp. 855–872, 2020.
- [72] X. Zhang, S. Qin, Y. Xu, and H. Xu, “Quaternion product units for deep learning on 3d rotation groups,” in *Conference on Computer Vision and Pattern Recognition*, 2020, pp. 7304–7313.
- [73] K. Shoemake, “Animating rotation with quaternion curves,” in *ACM Transactions on Graphics (Proceedings of SIGGRAPH)*, 1985, pp. 245–254.
- [74] Y. Zhou, C. Barnes, J. Lu, J. Yang, and H. Li, “On the continuity of rotation representations in neural networks,” in *Conference on Computer Vision and Pattern Recognition*, 2019, pp. 5745–5753.
- [75] S. Hampali, M. Rad, M. Oberweger, and V. Lepetit, “Honnotate: A method for 3d annotation of hand and object poses,” in *Conference on Computer Vision and Pattern Recognition*, 2020.
- [76] A. Knapitsch, J. Park, Q.-Y. Zhou, and V. Koltun, “Tanks and temples: Benchmarking large-scale scene reconstruction,” *ACM Transactions on Graphics*, 2017.
- [77] A. Kanazawa, J. Y. Zhang, P. Felsen, and J. Malik, “Learning 3d human dynamics from video,” in *Conference on Computer Vision and Pattern Recognition*, 2019, pp. 5614–5623.
- [78] A. Paszke, S. Gross, S. Chintala, G. Chanan, E. Yang, Z. DeVito, Z. Lin, A. Desmaison, L. Antiga, and A. Lerer, “Automatic differentiation in pytorch,” in *Neural Information Processing Systems Workshops*, 2017.
- [79] D. P. Kingma and J. Ba, “Adam: A method for stochastic optimization,” in *International Conference for Learning Representations*, 2014.
- [80] G. Moon and K. M. Lee, “I2l-meshnet: Image-to-lixel prediction network for accurate 3d human pose and mesh estimation from a single rgb image,” in *European Conference on Computer Vision*, 2020.

## REFERENCES

- [1] H. Lee, M. Billinghurst, and W. Woo, “Two-handed tangible interaction techniques for composing augmented blocks,” *Virtual Reality*, vol. 15, no. 2-3, pp. 133–146, 2011.

- [2] N. C. Camgoz, S. Hadfield, O. Koller, H. Ney, and R. Bowden, "Neural sign language translation," in *Conference on Computer Vision and Pattern Recognition*, 2018, pp. 7784–7793.
- [3] N. C. Camgoz, O. Koller, S. Hadfield, and R. Bowden, "Sign language transformers: Joint end-to-end sign language recognition and translation," in *Conference on Computer Vision and Pattern Recognition*, 2020, pp. 10023–10033.
- [4] M. Höll, M. Oberweger, C. Arth, and V. Lepetit, "Efficient physics-based implementation for realistic hand-object interaction in virtual reality," in *Conference on Virtual Reality and 3D User Interfaces*, 2018.
- [5] M. Parelli, K. Papadimitriou, G. Potamianos, G. Pavlakos, and P. Maragos, "Exploiting 3d hand pose estimation in deep learning-based sign language recognition from rgb videos," in *European Conference on Computer Vision*. Springer, 2020.
- [6] Z. Tu, H. Li, D. Zhang, J. Dauwels, B. Li, and J. Yuan, "Action-stage emphasized spatiotemporal vlad for video action recognition," *IEEE Transactions on Image Processing*, vol. 28, no. 6, pp. 2799–2812, 2019.
- [7] L. Ge, H. Liang, J. Yuan, and D. Thalmann, "Robust 3d hand pose estimation from single depth images using multi-view cnns," *IEEE Transactions on Image Processing*, vol. 27, no. 9, pp. 4422–4436, 2018.
- [8] Z. Yu, J. S. Yoon, I. K. Lee, P. Venkatesh, J. Park, J. Yu, and H. S. Park, "Humbi: A large multiview dataset of human body expressions," in *Conference on Computer Vision and Pattern Recognition*, 2020, pp. 2990–3000.
- [9] Z. Zhao, T. Wang, S. Xia, and Y. Wang, "Hand-3d-studio: A new multi-view system for 3d hand reconstruction," in *IEEE International Conference on Acoustics, Speech, and Signal Processing*. IEEE, 2020, pp. 2478–2482.
- [10] G. Poier, D. Schinagl, and H. Bischof, "Learning pose specific representations by predicting different views," in *Conference on Computer Vision and Pattern Recognition*, 2018, pp. 60–69.
- [11] A. Armagan, G. Garcia-Hernando, S. Baek, S. Hampali, M. Rad, Z. Zhang, S. Xie, M. Chen, B. Zhang, F. Xiong et al., "Measuring generalisation to unseen viewpoints, articulations, shapes and objects for 3d hand pose estimation under hand-object interaction," in *European Conference on Computer Vision*, 2020.
- [12] Y. Chen, Z. Tu, L. Ge, D. Zhang, R. Chen, and J. Yuan, "So-handnet: Self-organizing network for 3d hand pose estimation with semi-supervised learning," in *International Conference on Computer Vision*, 2019.
- [13] L. Ge, H. Liang, J. Yuan, and D. Thalmann, "Robust 3d hand pose estimation in single depth images: from single-view cnn to multi-view cnns," in *Conference on Computer Vision and Pattern Recognition*, 2016.
- [14] L. Huang, J. Tan, J. Liu, and J. Yuan, "Hand-transformer: Non-autoregressive structured modeling for 3d hand pose estimation," in *European Conference on Computer Vision*, 2020.
- [15] S. Yuan, G. Garcia-Hernando, B. Stenger, G. Moon, J. Yong Chang, K. Mu Lee, P. Molchanov, J. Kautz, S. Honari, L. Ge et al., "Depth-based 3d hand pose estimation: From current achievements to future goals," in *Conference on Computer Vision and Pattern Recognition*, 2018.
- [16] V. Athitsos and S. Sclaroff, "Estimating 3d hand pose from a cluttered image," in *Conference on Computer Vision and Pattern Recognition*, 2003.
- [17] Y. Cai, L. Ge, J. Cai, and J. Yuan, "Weakly-supervised 3d hand pose estimation from monocular rgb images," in *European Conference on Computer Vision*, 2018.
- [18] U. Iqbal, P. Molchanov, T. Breuel Juergen Gall, and J. Kautz, "Hand pose estimation via latent 2.5 d heatmap regression," in *European Conference on Computer Vision*, 2018.
- [19] A. Spurr, U. Iqbal, P. Molchanov, O. Hilliges, and J. Kautz, "Weakly supervised 3d hand pose estimation via biomechanical constraints," in *European Conference on Computer Vision*, 2020.
- [20] C. Zimmermann and T. Brox, "Learning to estimate 3d hand pose from single rgb images," in *International Conference on Computer Vision*, 2017.
- [21] L. Ge, Z. Ren, Y. Li, Z. Xue, Y. Wang, J. Cai, and J. Yuan, "3d hand shape and pose estimation from a single rgb image," in *Conference on Computer Vision and Pattern Recognition*, 2019.
- [22] D. Kulon, R. A. Guler, I. Kokkinos, M. M. Bronstein, and S. Zafeiriou, "Weakly-supervised mesh-convolutional hand reconstruction in the wild," in *Conference on Computer Vision and Pattern Recognition*, 2020.
- [23] Y. Hasson, B. Tekin, F. Bogo, I. Laptev, M. Pollefeys, and C. Schmid, "Leveraging photometric consistency over time for sparsely supervised hand-object reconstruction," in *Conference on Computer Vision and Pattern Recognition*, 2020.
- [24] Y. Hasson, G. Varol, D. Tzionas, I. Kalevatykh, M. J. Black, I. Laptev, and C. Schmid, "Learning joint reconstruction of hands and manipulated objects," in *Conference on Computer Vision and Pattern Recognition*, 2019.
- [25] N. Qian, J. Wang, F. Mueller, F. Bernard, V. Golyanik, and C. Theobalt, "Parametric hand texture model for 3d hand reconstruction and personalization," in *European Conference on Computer Vision*. Springer, 2020.
- [26] Z. Cao, T. Simon, S.-E. Wei, and Y. Sheikh, "Openpose: Realtime multi-person 2d pose estimation using part affinity fields." *IEEE Transactions on Pattern Analysis and Machine Intelligence*, 2019.
- [27] Y. Chen, Z. Tu, D. Kang, L. Bao, Y. Zhang, X. Zhe, R. Chen, and J. Yuan, "Model-based 3d hand reconstruction via self-supervised learning," in *Conference on Computer Vision and Pattern Recognition*, 2021, pp. 10451–10460.
- [28] Y. Cai, L. Ge, J. Cai, N. Magnenat-Thalmann, and J. Yuan, "3d hand pose estimation using synthetic data and weakly labeled rgb images," *IEEE Transactions on Pattern Analysis and Machine Intelligence*, 2020.
- [29] L. Yang and A. Yao, "Disentangling latent hands for image synthesis and pose estimation," in *Conference on Computer Vision and Pattern Recognition*, 2019, pp. 9877–9886.
- [30] K. Lin, L. Wang, and Z. Liu, "End-to-end human pose and mesh reconstruction with transformers," in *Conference on Computer Vision and Pattern Recognition*, 2021, pp. 1954–1963.
- [31] P. Chen, Y. Chen, D. Yang, F. Wu, Q. Li, Q. Xia, and Y. Tan, "I2uv-handnet: Image-to-uv prediction network for accurate and high-fidelity 3d hand mesh modeling," in *International Conference on Computer Vision*, 2021, pp. 12929–12938.
- [32] S. Liu, H. Jiang, J. Xu, S. Liu, and X. Wang, "Semi-supervised 3d hand-object poses estimation with interactions in time," in *Conference on Computer Vision and Pattern Recognition*, 2021, pp. 14687–14697.
- [33] Y. Zhou, M. Habermann, I. Habibie, A. Tewari, C. Theobalt, and F. Xu, "Monocular real-time full body capture with inter-part correlations," in *Conference on Computer Vision and Pattern Recognition*, 2021, pp. 4811–4822.
- [34] X. Chen, Y. Liu, C. Ma, J. Chang, H. Wang, T. Chen, X. Guo, P. Wan, and W. Zheng, "Camera-space hand mesh recovery via semantic aggregation and adaptive 2d-1d registration," in *Conference on Computer Vision and Pattern Recognition*, 2021, pp. 13274–13283.
- [35] Z. Cao, I. Radosavovic, A. Kanazawa, and J. Malik, "Reconstructing hand-object interactions in the wild," in *International Conference on Computer Vision*, October 2021, pp. 12417–12426.
- [36] D. Kulon, R. A. Guler, I. Kokkinos, M. M. Bronstein, and S. Zafeiriou, "Weakly-supervised mesh-convolutional hand reconstruction in the wild," in *Conference on Computer Vision and Pattern Recognition*, 2020, pp. 4990–5000.
- [37] I. Lim, A. Dielen, M. Campen, and L. Kobbelt, "A simple approach to intrinsic correspondence learning on unstructured 3d meshes," in *European Conference on Computer Vision*, 2018, pp. 0–0.
- [38] D. Kulon, H. Wang, R. A. Güler, M. M. Bronstein, and S. Zafeiriou, "Single image 3d hand reconstruction with mesh convolutions," in *British Machine Vision Conference*, 2019.
- [39] M. Defferrard, X. Bresson, and P. Vandergheynst, "Convolutional neural networks on graphs with fast localized spectral filtering," *Advances in neural information processing systems*, vol. 29, pp. 3844–3852, 2016.
- [40] L. Ge, Z. Ren, Y. Li, Z. Xue, Y. Wang, J. Cai, and J. Yuan, "3d hand shape and pose estimation from a single rgb image," in *Conference on Computer Vision and Pattern Recognition*, 2019, pp. 10833–10842.
- [41] J. Romero, D. Tzionas, and M. J. Black, "Embodied hands: Modeling and capturing hands and bodies together," *ACM Transactions on Graphics*, 2017.
- [42] A. Boukhayma, R. d. Bem, and P. H. Torr, "3d hand shape and pose from images in the wild," in *Conference on Computer Vision and Pattern Recognition*, 2019, pp. 10843–10852.
- [43] Y. Chen, Z. Tu, D. Kang, R. Chen, L. Bao, Z. Zhang, and J. Yuan, "Joint hand-object 3d reconstruction from a single image with cross-branch feature fusion," *IEEE Transactions on Image Processing*, 2020.

- [44] C. Zimmermann, D. Ceylan, J. Yang, B. Russell, M. Argus, and T. Brox, "Freihand: A dataset for markerless capture of hand pose and shape from single rgb images," in *International Conference on Computer Vision*, 2019.
- [45] S. Baek, K. I. Kim, and T.-K. Kim, "Pushing the envelope for rgb-based dense 3d hand pose estimation via neural rendering," in *Conference on Computer Vision and Pattern Recognition*, 2019.
- [46] —, "Weakly-supervised domain adaptation via gan and mesh model for estimating 3d hand poses interacting objects," in *Conference on Computer Vision and Pattern Recognition*, 2020, pp. 6121–6131.
- [47] J. Wang, F. Mueller, F. Bernard, S. Sorli, O. Sotnychenko, N. Qian, M. A. Otaduy, D. Casas, and C. Theobalt, "RGB2Hands: Real-Time Tracking of 3D Hand Interactions from Monocular RGB Video," *ACM Transactions on Graphics (Proceedings of SIGGRAPH Asia)*, 2020.
- [48] Y. Zhou, M. Habermann, W. Xu, I. Habibie, C. Theobalt, and F. Xu, "Monocular real-time hand shape and motion capture using multi-modal data," in *Conference on Computer Vision and Pattern Recognition*, 2020.
- [49] P. Panteleris, I. Oikonomidis, and A. Argyros, "Using a single rgb frame for real time 3d hand pose estimation in the wild," in *Winter Conference on Applications of Computer Vision*, 2018.
- [50] S. Wu, C. Rupprecht, and A. Vedaldi, "Unsupervised learning of probably symmetric deformable 3d objects from images in the wild," in *Conference on Computer Vision and Pattern Recognition*, 2020.
- [51] S. Goel, A. Kanazawa, and J. Malik, "Shape and viewpoint without keypoints," in *European Conference on Computer Vision*, 2020.
- [52] C. Wan, T. Probst, L. V. Gool, and A. Yao, "Self-supervised 3d hand pose estimation through training by fitting," in *Conference on Computer Vision and Pattern Recognition*, 2019.
- [53] Y. Chen, F. Wu, Z. Wang, Y. Song, Y. Ling, and L. Bao, "Self-supervised learning of detailed 3d face reconstruction," *IEEE Transactions on Image Processing*, vol. 29, pp. 8696–8705, 2020.
- [54] A. Tewari, M. Zollhöfer, P. Garrido, F. Bernard, H. Kim, P. Pérez, and C. Theobalt, "Mofa: Self-supervised multi-level face model learning for monocular reconstruction at over 250 hz," in *Conference on Computer Vision and Pattern Recognition*, 2018.
- [55] A. Tewari, M. Zollhöfer, H. Kim, P. Garrido, F. Bernard, P. Perez, and C. Theobalt, "Mofa: Model-based deep convolutional face autoencoder for unsupervised monocular reconstruction," in *International Conference on Computer Vision Workshops*, 2017.
- [56] V. Blanz and T. Vetter, "A morphable model for the synthesis of 3d faces," in *ACM Transactions on Graphics (Proceedings of SIGGRAPH)*, 1999, pp. 187–194.
- [57] M. de La Gorce, D. J. Fleet, and N. Paragios, "Model-based 3d hand pose estimation from monocular video," *IEEE Transactions on Pattern Analysis and Machine Intelligence*, 2011.
- [58] M. de La Gorce, N. Paragios, and D. J. Fleet, "Model-based hand tracking with texture, shading and self-occlusions," in *Conference on Computer Vision and Pattern Recognition*, 2008.
- [59] Y. Cai, L. Ge, J. Liu, J. Cai, T.-J. Cham, J. Yuan, and N. M. Thalmann, "Exploiting spatial-temporal relationships for 3d pose estimation via graph convolutional networks," in *International Conference on Computer Vision*, 2019, pp. 2272–2281.
- [60] J. Yang, H. J. Chang, S. Lee, and N. Kwak, "Seqhand: Rgb-sequence-based 3d hand pose and shape estimation," in *European Conference on Computer Vision*. Springer, 2020, pp. 122–139.
- [61] K. Fragkiadaki, S. Levine, P. Felsen, and J. Malik, "Recurrent network models for human dynamics," in *International Conference on Computer Vision*, 2015, pp. 4346–4354.
- [62] J. Martinez, M. J. Black, and J. Romero, "On human motion prediction using recurrent neural networks," in *Conference on Computer Vision and Pattern Recognition*, 2017, pp. 2891–2900.
- [63] E. Aksan, M. Kaufmann, and O. Hilliges, "Structured prediction helps 3d human motion modelling," in *International Conference on Computer Vision*, 2019, pp. 7144–7153.
- [64] A. Hernandez, J. Gall, and F. Moreno-Noguer, "Human motion prediction via spatio-temporal inpainting," in *International Conference on Computer Vision*, 2019, pp. 7134–7143.
- [65] M. Tan and Q. V. Le, "Efficientnet: Rethinking model scaling for convolutional neural networks," in *International Conference on Machine Learning*, 2019.
- [66] H. Kato, Y. Ushiku, and T. Harada, "Neural 3d mesh renderer," in *Conference on Computer Vision and Pattern Recognition*, 2018.
- [67] A. Newell, K. Yang, and J. Deng, "Stacked hourglass networks for human pose estimation," in *European Conference on Computer Vision*, 2016.
- [68] X. Sun, B. Xiao, F. Wei, S. Liang, and Y. Wei, "Integral human pose regression," in *European Conference on Computer Vision*, 2018.
- [69] P. J. Huber, "Robust estimation of a location parameter," in *Breakthroughs in statistics*. Springer, 1992, pp. 492–518.
- [70] Z. Wang, A. C. Bovik, H. R. Sheikh, and E. P. Simoncelli, "Image quality assessment: from error visibility to structural similarity," *IEEE Transactions on Image Processing*, 2004.
- [71] D. Pavlo, C. Feichtenhofer, M. Auli, and D. Grangier, "Modeling human motion with quaternion-based neural networks," *International Journal of Computer Vision*, vol. 128, no. 4, pp. 855–872, 2020.
- [72] X. Zhang, S. Qin, Y. Xu, and H. Xu, "Quaternion product units for deep learning on 3d rotation groups," in *Conference on Computer Vision and Pattern Recognition*, 2020, pp. 7304–7313.
- [73] K. Shoemake, "Animating rotation with quaternion curves," in *ACM Transactions on Graphics (Proceedings of SIGGRAPH)*, 1985, pp. 245–254.
- [74] Y. Zhou, C. Barnes, J. Lu, J. Yang, and H. Li, "On the continuity of rotation representations in neural networks," in *Conference on Computer Vision and Pattern Recognition*, 2019, pp. 5745–5753.
- [75] S. Hampali, M. Rad, M. Oberweger, and V. Lepetit, "Honnotate: A method for 3d annotation of hand and object poses," in *Conference on Computer Vision and Pattern Recognition*, 2020.
- [76] A. Knapitsch, J. Park, Q.-Y. Zhou, and V. Koltun, "Tanks and temples: Benchmarking large-scale scene reconstruction," *ACM Transactions on Graphics*, 2017.
- [77] A. Kanazawa, J. Y. Zhang, P. Felsen, and J. Malik, "Learning 3d human dynamics from video," in *Conference on Computer Vision and Pattern Recognition*, 2019, pp. 5614–5623.
- [78] A. Paszke, S. Gross, S. Chintala, G. Chanan, E. Yang, Z. DeVito, Z. Lin, A. Desmaison, L. Antiga, and A. Lerer, "Automatic differentiation in pytorch," in *Neural Information Processing Systems Workshops*, 2017.
- [79] D. P. Kingma and J. Ba, "Adam: A method for stochastic optimization," in *International Conference for Learning Representations*, 2014.
- [80] G. Moon and K. M. Lee, "I2l-meshnet: Image-to-lixel prediction network for accurate 3d human pose and mesh estimation from a single rgb image," in *European Conference on Computer Vision*, 2020.